Applying BCS–BEC crossover theory to high-temperature superconductors and ultracold atomic Fermi gases

(Review Article)

Qijin Chen[1], Jelena Stajic[2], and K. Levin[1]

[1]James Franck Institute and Department of Physics, University of Chicago
Chicago, Illinois, 60637 USA
E-mail: qchen@jfi.uchicaqo.edu

[2]Los Alamos National Laboratory, Los Alamos, New Mexico, 87545 USA

This review is written at the time of the twentieth anniversary of the discovery of high-temperature superconductors, which, nearly coincides with the important discovery of the superfluid phases of ultracold trapped fermionic atoms. We show how these two subjects have much in common. Both have been addressed from the perspective of the BCS–Bose–Einstein condensation (BEC) crossover scenario, which is designed to treat short coherence length superfluids with transition temperatures which are «high», with respect to the Fermi energy. A generalized mean field treatment of BCS–BEC crossover at general temperatures T, based on the BCS–Leggett ground state, has met with remarkable success in the fermionic atomic systems. Here we summarize this success in the context of four different cold atom experiments, all of which provide indications, direct or indirect, for the existence of a pseudogap. This scenario also provides a physical picture of the pseudogap phase in the underdoped cuprates which is a central focus of high T_c research. We summarize successful applications of BCS–BEC crossover to key experiments in high T_c systems including the phase diagram, specific heat, and vortex core STM data, along with the Nernst effect, and exciting recent data on the superfluid density in very underdoped samples.

1. Introduction

1.1. Historical background

Most workers in the field of high T_c superconductivity would agree that we have made enormous progress in the last 20 years in characterizing these materials and in identifying key theoretical questions and constructs. Experimental progress, in large part, comes from transport studies [1,2] in addition to three powerful spectroscopies: photoemission [3,4], neutron [5–12] and Josephson interferometry [13–15]. Over the last two decades, theorists have emphasized different aspects of the data, beginning with the anomalous normal state associated with the highest T_c systems («optimal doping») and next, establishing the nature and implications of the superconducting phase, which was ultimately revealed to have a d-wave symmetry. Now at the time of this twenty year anniversary, one of the most exciting areas of research involves the normal state again, but in the low T_c regime, where the system is «underdoped» and in proximity to the Mott insulating phase. We refer to this unusual phase as the «pseudogap state».

This pseudogap phase represents a highly anomalous form of superconductivity in the sense that there is an excitation gap present at the superfluid transition temperature T_c where long range order sets in. The community has struggled with two generic classes

of scenarios for explaining the pseudogap and its implications below T_c. Either the excitation gap is intimately connected to the superconducting order reflecting, for example, the existence of «pre-formed pairs», or it is extrinsic and associated with a competing ordered state unrelated to superconductivity.

The emphasis of this Review is on the pseudogap state as addressed by a particular preformed pair scenario which has its genesis in what is now referred to as «BEC–Bose–Einstein condensation (BEC) crossover theory». Here one contemplates that the attraction (of unspecified origin) which leads to superconductivity is stronger than in conventional superconductivity. In this way fermion pairs form before they Bose condense, much as in a Bose superfluid. In support of this viewpoint for the cuprates are the observations that: (i) the coherence length ξ for superconductivity is anomalously short, around 10 Å as compared with 1000 Å for a typical superconductor. Moreover (ii) the transition temperatures are anomalously high, and (iii) the systems are close to two-dimensional (2D) (where pre-formed pair or fluctuation effects are expected to be important). Finally, (iv) the pseudogap has the same d-wave symmetry [16] as the superconducting order parameter [3,4] and there seems to be a smooth evolution of the excitation gap from above to below T_c.

To investigate this BCS–BEC crossover scenario we have the particular good fortune today of having a new class of atomic physics experiments involving ultracold trapped fermions which, in the presence of an applied magnetic field, have been found to have a continuously tunable attractive interaction. At high fields the system exhibits BCS-like superfluidity, whereas at low fields one sees BEC-like behavior.

This Review presents a consolidated study of both the pseudogap phase of the cuprates and recent developments in ultracold fermionic superfluids. The emphasis of these cold atom experiments is on the so-called unitary or strong scattering regime, which is between the BEC and BCS limits, but on the fermionic side. The superfluid state in this intermediate regime is also referred to in the literature as a «resonant superfluid» [17,18]. Here we prefer to describe it as the «pseudogap phase», since that is more descriptive of the physics and underlines the close analogy with high T_c systems. Throughout this Review we will use these three descriptive phrases interchangeably.

1.2. Fermionic pseudogaps and metastable pairs: two sides of the same coin

BCS–BEC crossover theory is based on the observations of Eagles [19] and Leggett [20] who independently noted that the BCS ground state wavefunction

$$\Psi_0 = \Pi_{\mathbf{k}}(u_k + v_{\mathbf{k}} c_k^{\dagger} c_{-k}^{\dagger})|0\rangle \qquad (1)$$

had a greater applicability than had been appreciated at the time of its original proposal by Bardeen, Cooper and Schrieffer (BCS). As the strength of the attractive pairing interaction U (< 0) between fermions is increased, this wavefunction is also capable of describing a continuous evolution from BCS like behavior to a form of BEC. What is essential is that the chemical potential μ of the fermions be self consistently computed as U varies.

The variational parameters $v_{\mathbf{k}}$ and $u_{\mathbf{k}}$ are usually represented by the two more directly accessible parameters $\Delta_{sc}(0)$ and μ, which characterize the fermionic system. Here $\Delta_{sc}(0)$ is the zero temperature superconducting order parameter. These fermionic parameters are uniquely determined in terms of U and the fermionic density n. The variationally determined self consistency conditions are given by two BCS-like equations which we refer to as the «gap» and «number» equations respectively:

$$\Delta_{sc}(0) = -U \sum_{\mathbf{k}} \Delta_{sc}(0) \frac{1}{2E_{\mathbf{k}}};$$

$$n = 2 \sum_{\mathbf{k}} \left[1 - \frac{\epsilon_{\mathbf{k}} - \mu}{E_{\mathbf{k}}} \right] \qquad (2)$$

where

$$E_{\mathbf{k}} \equiv \sqrt{(\epsilon_{\mathbf{k}} - \mu)^2 + \Delta_{sc}^2(0)} \qquad (3)$$

and $\epsilon_{\mathbf{k}} = \hbar^2 k^2 / 2m$ are the dispersion relations for the Bogoliubov quasiparticles and free fermions, respectively. An additional advantage of this formalism is that Bogoliubov–de Gennes theory, a real space implementation of this ground state, can be used to address the effects of inhomogeneity and external fields at $T = 0$. This has been widely used in the crossover literature.

Within this ground state there have been extensive studies [21] of collective modes [22,23] and effects of two dimensionality [22]. Nozieres and Schmitt–Rink were the first [24] to address non-zero T. We will outline some of their conclusions later in this Review. Randeria and co-workers reformulated the approach of Nozieres and Schmitt–Rink (NSR) and moreover, raised the interesting possibility that crossover physics might be relevant to high-temperature superconductors [22]. Subsequently other workers have applied this picture to the high T_c cuprates [25–27] and ultracold fermions [17,18,28,29] as well as formulated alternative schemes [30,31] for addressing $T \neq 0$. Importantly, a number of experimentalists, most notably Uemura [32], have claimed evidence in support [33–35] of the BCS–BEC crossover picture for high T_c materials.

Compared to work on the ground state, considerably less has been written on crossover effects at non-zero temperature based on Eq. (1). Because our understanding has increased substantially since the pioneering work of NSR, and because they are the most interesting, this review is focused on these finite T effects.

The importance of obtaining a generalization of BCS theory which addresses the crossover from BCS to BEC ground state at temperatures $T \leq T_c$ cannot be overestimated. BCS theory as originally postulated can be viewed as a paradigm among theories of condensed matter systems; it is complete, in many ways generic and model independent, and well verified experimentally. The observation that the wavefunction of Eq. (1) goes beyond strict BCS theory, suggests that there is a larger mean field theory to be addressed. Equally exciting is the possibility that this mean field theory can be discovered and simultaneously tested in a very controlled fashion using ultracold fermionic atoms [17,18]. Mean field approaches are always approximate. We can ascribe the simplicity and precision of BCS theory to the fact that in conventional superconductors the coherence length ξ is extremely long. As a result, the kind of averaging procedure implicit in mean field theory becomes nearly exact. Once ξ becomes small BCS is not expected to work at the same level of precision. Nevertheless even when they are not exact, mean field approaches are excellent ways of building up intuition. And further progress is not likely to be made without investigating first the simplest of mean field approaches, associated with Eq. (1).

The effects of BEC–BCS crossover are most directly reflected in the behavior of the fermionic chemical potential μ. We plot the behavior of $\mu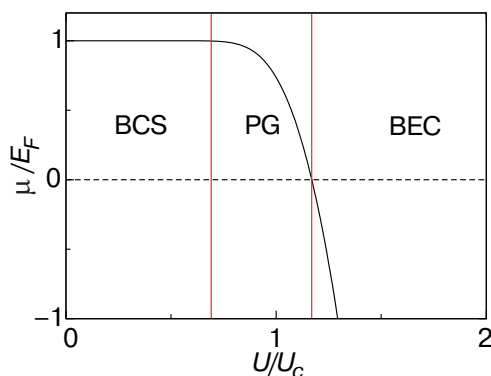$ in Fig. 1, which indicates the BCS and BEC regimes. In the weak coupling regime $\mu = E_F$ and ordinary BCS theory results. However at sufficiently strong coupling, μ begins to decrease, eventually crossing zero and then ultimately becoming negative in the BEC regime, with increasing $|U|$. We generally view $\mu = 0$ as a crossing point. For positive μ the system has a remnant of a Fermi surface, and we say that it is «fermionic». For negative μ, the Fermi surface is gone and the material is «bosonic».

The new and largely unexplored physics of this problem lies in the fact that once outside the BCS regime, but before BEC, superconductivity or superfluidity emerge out of a very exotic, non-Fermi liquid normal state. Emphasized in Fig. 1 is this intermediate (i.e., pseudogap or PG) regime having positive μ which we associate with non-Fermi liquid based superconductivity [25,36,37]. Here, the onset of superconductivity occurs in the presence of fermion pairs. Unlike their counterparts in the BEC limit, these pairs are not infinitely long lived. Their presence is apparent even in the normal state where an energy must be applied to create fermionic excitations. This energy cost derives from the breaking of the metastable pairs. Thus we say that there is a «pseudogap» (PG) at and above T_c. It will be stressed throughout this Review that gaps in the fermionic spectrum and bosonic degrees of freedom are two sides of the same coin. A particularly important observation to make is that the starting point for crossover physics is based on the fermionic degrees of freedom. A non-zero value of the excitation gap Δ is equivalent to the presence of metastable or stable fermion pairs. And it is only in this indirect fashion that we can probe the presence of these «bosons», within the framework of Eq. (1).

In many ways this crossover theory appears to represent a more generic form of superfluidity. Without doing any calculations we can anticipate some of the effects of finite temperature. Except for very weak coupling, *pairs form and condense at different temperatures.* More generally, in the presence of a moderately strong attractive interaction it pays energetically to take some advantage and to form pairs (say roughly at temperature T^*) within the normal state. Then, for statistical reasons these bosonic degrees of freedom ultimately are driven to condense at $T_c < T^*$, as in BEC.

Just as there is a distinction between T_c and T^*, *there must be a distinction between the superconducting order parameter Δ_{sc} and the excitation gap Δ.* In Fig. 2 we present a schematic plot of these two energy parameters. It may be seen that the order parameter vanishes at T_c, as in a second order phase transition, while the excitation gap turns on smoothly below T^*. It should also be stressed that there is only one gap
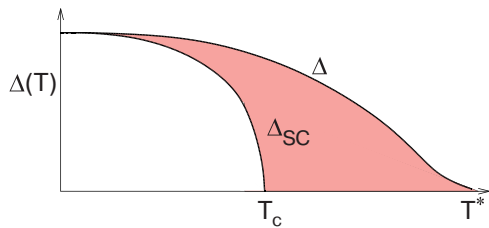

Fig. 1. Behavior of the $T = 0$ chemical potential μ in the three regimes. μ is essentially pinned at the Fermi temperature E_F in the BCS regime, whereas it becomes negative in the BEC regime. The PG (pseudogap) case corresponds to non-Fermi liquid based superconductivity in the intermediate regime.

Fig. 2. Contrasting behavior of the excitation gap $\Delta(T)$ and order parameter $\Delta_{sc}(T)$ versus temperature in the pseudogap regime. The height of the shaded region reflects the number of noncondensed pairs, at each temperature.

energy scale in the ground state [20] of Eq. (1). Thus $\Delta_{sc}(0) = \Delta(0)$.

In addition to the distinction between Δ and Δ_{sc}, another important way in which *bosonic degrees of freedom are revealed is indirectly through the temperature dependence of Δ. In the BEC regime where fermionic pairs are pre-formed, Δ is essentially constant for all $T \leq T_c$ (as is μ).* By contrast in the BCS regime it exhibits the well known temperature dependence of the superconducting order parameter. This behavior is illustrated in Fig. 3.

Again, without doing any calculations we can make one more inference about the nature of crossover physics at finite T. *The excitations of the system must smoothly evolve from fermionic in the BCS regime to bosonic in the BEC regime.* In the intermediate case, the excitations are a mix of fermions and metastable pairs. Figure 4 characterizes the excitations out of the condensate as well as in the normal phase. This schematic figure will play an important role in our thinking throughout this Review.
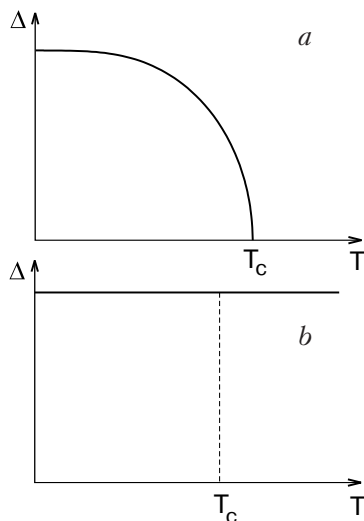

Fig. 3. Comparison of temperature dependence of excitation gaps in BCS (*a*) and BEC (*b*) limits. The gap vanishes at T_c for the former while it is essentially T-independent for the latter.

1.3. Introduction to high T_c superconductivity: pseudogap effects

This Review deals with the intersection of two fields and two important problems: high-temperature superconductors and ultracold fermionic atoms in which, through Feshbach resonance effects, the attractive interaction may be arbitrarily tuned by a magnetic field. Our focus is on the broken symmetry phase and how it evolves from the well known ground state at $T = 0$ to $T = T_c$. We begin with a brief overview [1,2] of pseudogap effects in high-temperature superconductors. There is an extensive body of theoretical literature which aims to understand these pseudogap effects from a variety of different viewpoints. We list some of these in Refs. 38–40 for the interested reader. A study of concrete data in these systems provides a rather natural way of building intuition about non-Fermi liquid based superfluidity, and this should, in turn, be useful for the cold atom community.

It has been argued by some [26,27,42–44] that a BCS–BEC crossover-induced pseudogap is the origin of the mysterious normal state gap observed in high-temperature superconductors. While this is a highly contentious subject some of the arguments in favor of this viewpoint (beyond those listed in Section 1.1) rest on the following observations: (i) To a good approximation the pseudogap onset temperature [45,46] $T^* \approx 2\Delta(0)/4.3$ which satisfies the BCS scaling relation. (ii) There is widespread evidence for pseudogap effects both above [1,2] as well as (iii) below [47,48] T_c. (iv) In addition, it has also been argued that short coherence length superconductors may quite generally exhibit a distinctive form of superconductivity [32] which sets them apart from conventional superconductors. One might want, then, to concentrate on this more generic feature (rather than on more exotic aspects), which they have in common with other superconductors in their distinctive class.
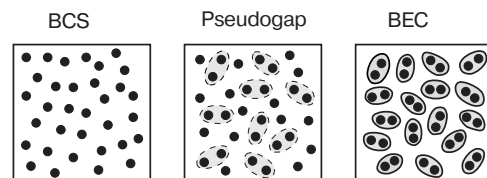

Fig. 4. The character of the excitations in the BCS–BEC crossover both above and below T_c. The excitations are primarily fermionic Bogoliubov quasiparticles in the BCS limit and bosonic pairs (or «Feshbach bosons») in the BEC limit. For atomic Fermi gases, the «virtual molecules» in the PG case consist primarily of «Cooper» pairs of fermionic atoms.

In Fig. 5 we show a sketch of the phase diagram for the hole-doped copper oxide superconductors. Here x represents the concentration of holes which can be controlled by, say, adding Sr substitutionally to $L_{1-x}Sr_xCuO_4$. At zero and small x the system is an antiferromagnetic (AFM) insulator. Precisely at half filling ($x = 0$) we understand this insulator to derive from Mott effects. These Mott effects may or may not be the source of the other exotic phases indicated in the diagram, i.e., the superconducting (SC) and the «pseudogap» phases. Once AFM order disappears the system remains insulating until a critical hole concentration (typically around a few percent) when an insulator-superconductor transition is encountered. Here photoemission studies [3,4] suggest that once this line is crossed, μ appears to be positive. For $x \leq 0.2$, the superconducting phase has a non-Fermi liquid (or pseudogapped) normal state [2]. We note an important aspect of this phase diagram at low x. As the pseudogap becomes stronger (T^* increases), superconductivity as reflected in the magnitude of T_c becomes weaker.

Figure 6 indicates the temperature dependence of the excitation gap for three different hole stoichiometries. These data [3] were taken from angle resolved photoemission spectroscopy (ARPES) measurement. For one sample shown as circles, (corresponding roughly to «optimal» doping) the gap vanishes roughly at T_c as might be expected for a BCS superconductor. At the other extreme are the data indicated by inverted triangles in which an excitation gap appears to be present up to room temperature, with very little temperature dependence. This is what is referred to as a highly underdoped sample (small x), which from the phase diagram can be seen to have a rather
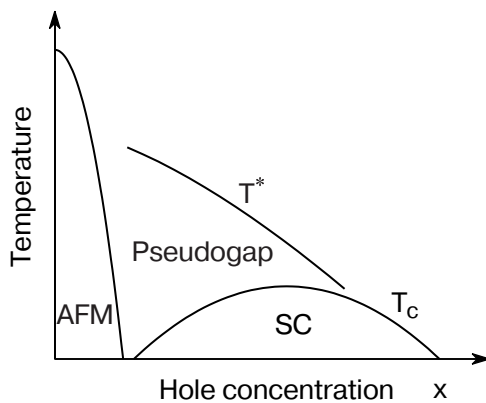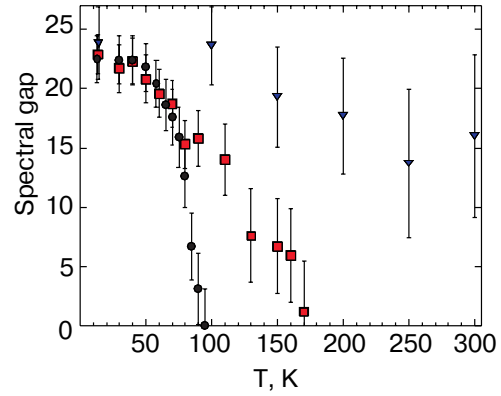

Fig. 6. Temperature dependence of the excitation gap at the antinodal point $(\pi,0)$ in $Bi_2Sr_2CaCu_2O_{8+\delta}$ (BSCCO) for three different doping concentrations from near-optimal (discs) to heavy underdoping (inverted triangles), as measured by angle-resolved photoemission spectroscopy (from Ref. 3).

low T_c. Moreover, T_c is not evident in these data on underdoped samples.

While the high T_c community has focused on pseudogap effects above T_c, there is a good case to be made that these effects also persist below. STM data [33] taken below T_c within a vortex core indicate that there is a clear depletion of the density of states around the Fermi energy in the normal phase within the core. These data underline the fact that the existence of an energy gap has little or nothing to do with the existence of phase coherent superconductivity. It also underlines the fact that pseudogap effects effectively persist below T_c; the normal phase underlying superconductivity for $T \leq T_c$ is not a Fermi liquid.

Analysis of thermodynamical data [2,47] has led to a similar inference. For the PG case, the entropy extrapolated into the superfluid phase, based on Fermi liquid theory, becomes negative. In this way Loram and co-workers [47] deduced that the normal phase underlying the superconducting state is not a Fermi liquid. Rather, they claimed to obtain proper thermodynamics, it must be assumed that this state contains a persistent pseudogap. In this way they argued for a distinction between the excitation gap Δ and the superconducting order parameter, within the superconducting phase. To fit their data they presume a modified fermionic dispersion $E_{\mathbf{k}} = \sqrt{(\epsilon_{\mathbf{k}} - \mu)^2 + \Delta^2(T)}$ where

$$\Delta^2(T) = \Delta^2_{sc}(T) + \Delta^2_{pg} \qquad (4)$$

Here Δ_{pg} is taken on phenomenological grounds to be T-independent. While Eq. (4) is also found in BCS–BEC crossover theory, there are important differences. In the latter approach $\Delta_{pg} \rightarrow 0$ as $T \rightarrow 0$.

Fig. 5. Typical phase diagram of hole-doped high T_c superconductors. The horizontal axis is hole doping concentration. There exists a pseudogap phase above T_c in the underdoped regime. Here SC denotes superconductor, and T^* is the temperature at which the pseudogap smoothly turns on.

Finally, Fig. 7 makes the claim for a persistent pseudogap below T_c in an even more suggestive way. Figure 7,*a* represents a schematic plot of excitation gap data such as are shown in Fig. 6. Here the focus is on temperatures below T_c. Most importantly, this figure indicates that the T dependence in Δ varies dramatically as the stoichiometry changes. Thus, in the extreme underdoped regime, where PG effects are most intense, there is very little T dependence in Δ below T_c. By contrast at high x, when PG effects are less important, the behavior of Δ follows that of BCS theory. What is most impressive however, is that these wide variations in $\Delta(T)$ are *not* reflected in the superfluid density $\rho_s(T)$. Figure 7 then indicates that, *despite the highly non-universal behavior for $\Delta(T)$, the superfluid density does not make large excursions from its BCS- predicted form*. This is difficult to understand if the fermionic degrees of freedom through $\Delta(T)$ are dominating at all x. Rather this figure suggests that something other than fermionic excitations is responsible for the disappearance of superconductivity, particularly in the regime where $\Delta(T)$ is relatively constant in T. At the very least pseudogap effects must persist below T_c.

The phase diagram also suggests that pseudogap effects become stronger with underdoping. How does one accommodate this in the BCS—BEC crossover scenario? At the simplest level one may argue that as the system approaches the Mott insulating limit, fermions are less mobile and the effectiveness of the attraction increases. In making the connection between the strength of the attraction and the variable x in the cuprate phase diagram we will argue that it is appropriate to simply fit $T^*(x)$. In this Review we do not emphasize Mott physics because it is not particularly relevant to the atomic physics problem. It also seems to be complementary to the BCS—BEC crossover scenario. It is understood that both components are important in high T_c superconductivity. It should be stressed that hole concentration x in the cuprates plays the role of applied magnetic field in the cold atom system. These are the external parameters which serve to tune the BCS—BEC crossover.

Is there any evidence for bosonic degrees of freedom in the normal state of high T_c superconductors? The answer is unequivocally yes: *metastable bosons are observable as superconducting fluctuations*. These effects are enhanced in the presence of the quasi-two-dimensional lattice structure of these materials. In the underdoped case, one can think of T^* as marking the onset of preformed pairs which are closely related to fluctuations of conventional superconductivity theory, but which are made more robust as a result of BCS—BEC crossover effects, that is, stronger pairing attraction. A number of people have argued [49,50] that fluctuating normal state vortices are responsible for the anomalous transport behavior of the pseudogap regime. It has been proposed [51] that these data may alternatively be interpreted as suggesting that bosonic degrees of freedom are present in the normal state.
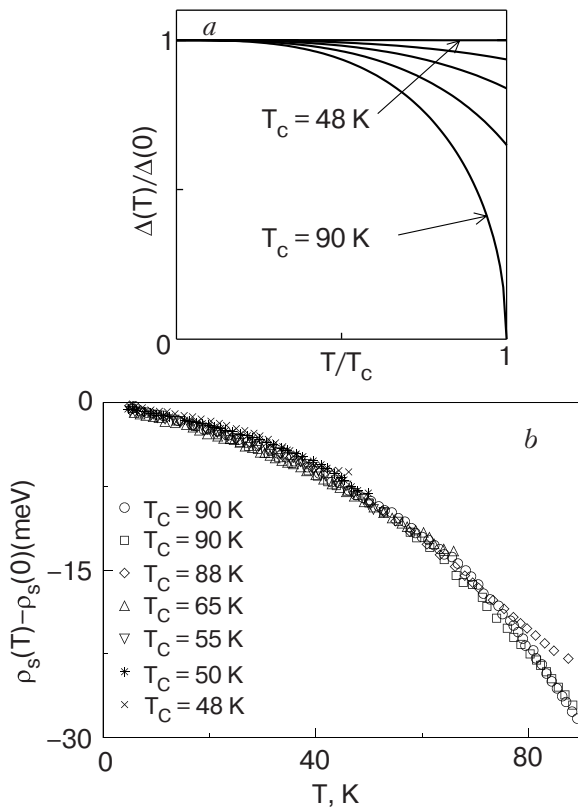

Fig. 7. Temperature dependence of fermionic excitation gaps Δ and superfluid density ρ_s for various doping concentrations (from Ref. 48). When $\Delta(T_c) \neq 0$, there is little correlation between $\Delta(T)$ and $\rho_s(T)$; this figure suggests that something other than fermionic quasiparticles (e.g., bosonic excitations) may be responsible for the disappearance of superconductivity with increasing T. Figure (*b*) shows a quasi-universal behavior for the slope $d\rho_s/dT$ at different doping concentrations, despite the highly non-universal behavior for $\Delta(T)$.

1.4. Summary of cold atom experiments: crossover in the presence of Feshbach resonances

There has been an exciting string of developments over the past few years in studies of ultracold fermionic atoms, in particular, ^{6}Li and ^{40}K, which have been trapped and cooled via magnetic and optical means. Typically these traps contain 10^5 atoms at very low densities $\approx 10^{13}$ cm^{-3}. Here the Fermi temperature in a trap can be estimated to be of the order of a microkelvin. It was argued on the basis of BCS theory alone [52], and rather early on (1997), that the temperatures associated with the superfluid phases may be

attainable in these trapped gases. This set off a search for the «holy grail» of fermionic superfluidity. That a Fermi degenerate state could be reached at all is itself quite remarkable; this was first reported [53] by Jin and deMarco in 1999. By late 2002 reports of unusual hydrodynamics in a degenerate Fermi gas indicated that strong interactions were present [54]. This strongly interacting Fermi gas (associated with the unitary scattering regime) has attracted widespread attention independent of the search for superfluidity, because it appears to be a prototype for analogous systems in nuclear physics [55,56] and in quark-gluon plasmas [57,58]. Moreover, there has been a fairly extensive body of analytic work on the ground state properties of this regime [59,60], which goes beyond the simple mean field wave function ansatz.

As a consequence of attractive *s*-wave interactions between fermionic atoms in different hyperfine states, it was anticipated that dimers could also be made. Indeed, these molecules formed rather efficiently [62–64] as reported in mid-2003 either via three body recombination [65] or by sweeping the magnetic field across a Feshbach resonance. Moreover, they are extremely long lived [63]. From this work it was relatively straightforward to anticipate that a Bose condensate would also be achieved. Credit goes to theorists such as Holland [17] and to Griffin [29] and their co-workers for recognizing that the superfluidity need not be only associated with condensation of long lived bosons, but in fact could also derive, as in BCS, from fermion pairs. In this way, it was argued that a suitable tuning of the attractive interaction via Feshbach resonance effects, would lead to a realization of a BCS–BEC crossover.

By late 2003 to early 2004, four groups [61,66–68] had observed the «condensation of weakly bound molecules» (that is, on the $a_s > 0$ side of resonance), and shortly thereafter a number had also reported evidence for superfluidity on the BCS side [69–72]. The BEC side is the more straightforward since the presence of the superfluid is reflected in a bimodal distribution in the density profile. This is shown in Fig. 8 from Ref. 61, and is conceptually similar to the behavior for condensed Bose atoms [73]. On the BEC side but near resonance, the estimated T_c is about $0.3T_F$, with condensate overtions varying from 20 or so to nearly 100 . The condensate lifetimes are relatively long in the vicinity of resonance, and fall off rapidly as one goes deeper into the BEC. However, for $a_s < 0$ there is no clear expectation that the density profile will provide a signature of the superfluid phase.

These claims that superfluidity may have been achieved on the BCS side ($a_s < 0$) of resonance were viewed as particularly exciting. The atomic commu-
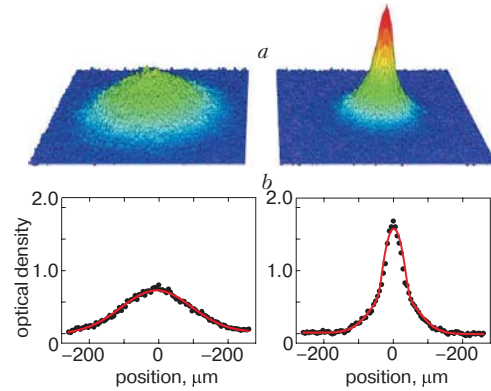

Fig. 8. Spatial density profiles of a molecular cloud of trapped ^{40}K atoms in the BEC regime in the transverse directions after 20 ms of free expansion (from Ref. 61), showing thermal molecular cloud above T_c (left) and a molecular condensate (right) below T_c. (*a*) shows the surface plots, and (*b*) shows the cross-sections through images (dots) with bimodal fits (lines).

nity, for the most part, felt the previous counterpart observations on the BEC side were expected and not significantly different from condensation in Bose atoms. The evidence for this new form of «fermionic superfluidity» rests on studies [69,70] that perform fast sweeps from negative a_s to positive a_s across the resonance. The field sweeps allow, in principle, a pairwise projection of fermionic atoms (on the BCS side) onto molecules (on the BEC side). It is presumed that in this way one measures the momentum distribution of fermion pairs. The existence of a condensate was thus inferred. Other experiments which sweep across the Feshbach resonance adiabatically, measure the size of the cloud after release [68] or within a trap [74].

Evidence for superfluidity on the BCS side, which does not rely on the sweep experiments, has also been deduced from collective excitations of a fermionic gas [71,75]. Pairing gap measurements with radio frequency (RF) spectroscopy probes [72] have similarly been interpreted [76] as providing support for the existence of superfluidity, although more directly these experiments establish the existence of fermion pairs. Quite recently, evidence for a phase transition has been presented via thermodynamic measurements and accompanying theory [77]. The latter, like the theory [76] of RF experiments [72], is based on the formalism presented in this Review. A most exciting and even more recent development has been the observation of vortices [78] which appears to provide a smoking gun for the existence of the superfluid phase.

2. Theoretical formalism for BCS−BEC crossover

2.1. Many-body Hamiltonian and two-body scattering theory

We introduce the Hamiltonian [17,29,79] used in the cold atom and high T_c crossover studies. The most general form for this Hamiltonian consists of two types of interaction effects: those associated with the direct interaction between fermions parametrized by U, and those associated with «fermion−boson» interactions, whose strength is governed by g.

$$H - \mu N =$$
$$= \sum_{\mathbf{k},\sigma}(\varepsilon_{\mathbf{k}} - \mu)a^{\dagger}_{\mathbf{k},\sigma}a_{\mathbf{k},\sigma} + \sum_{\mathbf{q}}(\epsilon^{mb}_{\mathbf{q}} + \nu - 2\mu)b^{\dagger}_{\mathbf{q}}b_{\mathbf{q}} +$$
$$+ \sum_{\mathbf{q},\mathbf{k},\mathbf{k}'}U(\mathbf{k},\mathbf{k}')a^{\dagger}_{\mathbf{q}/2+\mathbf{k},\uparrow}a^{\dagger}_{\mathbf{q}/2-\mathbf{k},\downarrow}a_{\mathbf{q}/2-\mathbf{k}',\downarrow}a_{\mathbf{q}/2+\mathbf{k}',\uparrow} +$$
$$+ \sum_{\mathbf{q},\mathbf{k}}(g(\mathbf{k})b^{\dagger}_{\mathbf{q}}a_{\mathbf{q}/2-\mathbf{k},\downarrow}a_{\mathbf{q}/2+\mathbf{k},\uparrow} + \mathrm{h.c.}). \tag{5}$$

Here the fermion and boson kinetic energies are given by $\epsilon_{\mathbf{k}} = k^2/2m$, and $\epsilon^{mb}_{\mathbf{q}} = q^2/2M$, and ν is an important parameter which represents the magnetic field-induced «detuning». Here we use the convention $\hbar = k_B = c = 1$. In this two channel problem the ground state wavefunction is slightly modified and given by

$$\overline{\Psi}_0 = \Psi_0 \otimes \Psi^B_0 \tag{6}$$

where the molecular or Feshbach boson contribution Ψ^B_0 is as given in Ref. 80.

Whether both forms of interactions are needed in either system is still under debate. The bosons ($b^{\dagger}_{\mathbf{k}}$) of the cold atom problem [17,18] are referred to as belonging to the «closed channel». These spin-singlet molecules represent a separate species, not to be confused with the («open channel») fermion pairs ($a^{\dagger}_{\mathbf{k}}a^{\dagger}_{-\mathbf{k}}$), which are associated with spin triplet. As a result of virtual occupation of the bound state of the closed channel the interaction between open channel fermions can be tuned (through applied magnetic field) to vary from weak to very strong.

In this review we will discuss the behavior of crossover physics both with and without the closed-channel. Previous studies of high T_c superconductors have invoked a similar bosonic term [27, 81−83] as well, although less is known about its microscopic origin. This fermion−boson coupling is not to be confused with the coupling between fermions and a «pairing-mechanism»-related boson ($[b + b^{\dagger}]a^{\dagger}a$) such as phonons in a metal superconductor. The coupling $b^{\dagger}aa$ and its Hermitian conjugate represent a form of sink and source for creating fermion pairs, in this way inducing superconductivity in some ways, as a by-product of Bose condensation.

It is useful at this stage to introduce the s-wave scattering length, a, defined by the low energy limit of two-body scattering in vacuum. We begin with the effects of U only, presuming that U is always an attractive interaction ($U < 0$) which can be arbitrarily varied,

$$\frac{m}{4\pi a} \equiv \frac{1}{U} + \sum_{\mathbf{k}}\frac{1}{2\epsilon_{\mathbf{k}}}. \tag{7}$$

We may define a critical value U_c of the potential as that associated with the binding of a two particle state in vacuum. We can write down an equation for U_c given by

$$U_c^{-1} = -\sum_{\mathbf{k}}\frac{1}{2\epsilon_{\mathbf{k}}} \tag{8}$$

although specific evaluation of U_c requires that there be a cut-off imposed on the above summation, associated with the range of the potential. *The fundamental postulate of crossover theory is that even though the two-body scattering length changes abruptly at the unitary scattering condition ($|a| = \infty$), in the N-body problem the superconductivity varies smoothly through this point.*

Provided we redefine the appropriate «two body» scattering length, Equation (7) holds even in the presence of Feshbach effects [28,29]. It has been shown that U in the above equations is replaced by

$$U \to U_{\mathrm{eff}} \equiv U + \frac{g^2}{2\mu - \nu} \tag{9}$$

and we write $a \to a^*$. Experimentally, the two-body scattering length a^* varies with magnetic field B. Thus we have

$$\frac{m}{4\pi a^*} \equiv \frac{1}{U_{\mathrm{eff}}} + \sum_{\mathbf{k}}\frac{1}{2\epsilon_{\mathbf{k}}}. \tag{10}$$

More precisely the effective interaction between two fermions is momentum and energy dependent. It arises from a second order process involving emission and absorption of a closed-channel molecular boson. The net effect of the direct plus indirect interactions is given by

$$\tilde{g}_{\mathrm{eff}}(Q,K,K') = g_{\mathrm{eff}}(Q)\varphi_{\mathbf{k}}\varphi_{\mathbf{k}'}$$
$$U_{\mathrm{eff}}(Q) \equiv U + g^2 D_0(Q),$$

where $D_0(Q) \equiv 1/[i\Omega_n - \epsilon^{mb}_{\mathbf{q}} - \nu + 2\mu]$ is the non-interacting molecular boson propagator. Here and throughout we use a four-momentum notation, $Q \equiv (\mathbf{q}, i\Omega_n)$, and its analytical continuation,

$Q \to (\mathbf{q}, \Omega + i0^+)$, and write $\Sigma_Q \equiv T \sum_{Q_n} \sum_{\mathbf{q}}$, where Ω_n is a Matsubara frequency. What appears in the gap equation, however, is $U_{\mathrm{eff}}(Q = 0)$ which we define to be U_{eff}. When the open-channel attraction U is weak, clearly, $2\mu \leq \nu$ is required so that the Feshbach-induced interaction is attractive. In the extreme BEC limit $\nu = 2\mu$. However, when a deep bound state exists in the open channel, such as in ^{40}K, the system may evolve into a metastable state such that $2\mu > \nu$ in the BEC regime and there is a point on the BCS side where $U_{\mathrm{eff}} = 0$ precisely.

Figure 9 presents a plot of this scattering length $k_F a_s \equiv k_F a^*$ for the case of ^{6}Li. It follows that a_s is negative when there is no bound state, it tends to $-\infty$ at the onset of the bound state and to $+\infty$ just as the bound state stabilizes. It remains positive but decreases in value as the interaction becomes increasingly strong. The magnitude of a_s is arbitrarily small in both the extreme BEC and BCS limits, but with opposite sign.

2.2. T-matrix-based approaches to BCS−BEC crossover in the absence of Feshbach effects

To address finite temperature in a way which is consistent with Eq. (1), or with alternative ground states, one introduces a T-matrix approach. Here one solves self consistently for the single fermion propagator G and the pair propagator t. That one stops at this level without introducing higher order Green's functions (involving three, and four particles, etc) is believed to be adequate for addressing a leading order mean field theory such as that represented by Eq. (1). One can see that pair−pair (boson−boson) interactions are only treated in a (generalized) mean field averaging procedure; they arise exclusively from the fermions and are sufficiently weak so as not to lead to any incomplete condensation in the ground state, as is compatible with Eq. (1).

In this section we demonstrate that at the T-matrix level there are three distinct schemes which can be im-
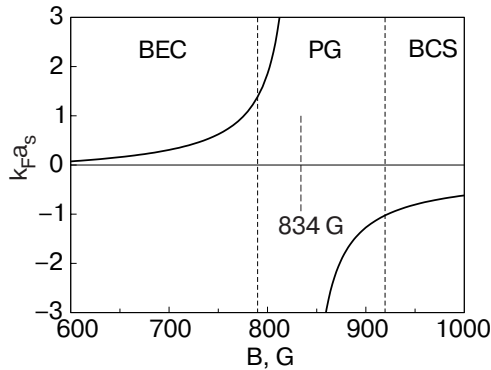
Fig. 9. Characteristic behavior of the scattering length for ^{6}Li in the three regimes.

plemented to address BCS−BEC crossover physics. Above T_c, quite generally one writes for the t-matrix

$$t(Q) = \frac{U}{1 + U\chi(Q)} \qquad (11)$$

and theories differ only on what is the nature of the pair susceptibility $\chi(Q)$, and the associated self energy of the fermions. Below T_c one can also consider a T-matrix approach to describe the particles and pairs in the condensate. For the most part we will defer extensions to the broken symmetry phase to Section 2.3.

In analogy with Gaussian fluctuations, Nozieres and Schmitt−Rink considered [24]

$$\chi_0(Q) = \sum_K G_0(K)G_0(Q - K) \qquad (12)$$

with self energy

$$\Sigma_0(K) = \sum_Q t(Q)G_0(Q - K), \qquad (13)$$

where $G_0(K)$ is the noninteracting fermion Green's function. The number equation of the Nozieres−Schmitt−Rink scheme [22,24] is then deduced in an approximate fashion [84] by using a leading order series for G with

$$G = G_0 + G_0\Sigma_0 G_0. \qquad (14)$$

It is straightforward, however, to avoid this approximation in Dyson's equation, and a number of groups [31,37] have extended NSR in this way.

Similarly one can consider

$$\bar{\chi}(Q) = \sum_K G(K)G(Q - K) \qquad (15)$$

with self energy

$$\bar{\Sigma}(K) = \sum_Q t(Q)G(Q - K). \qquad (16)$$

This latter scheme has been also extensively discussed in the literature, by among others, Haussmann [85], Tchernyshyov [86] and Yamada and Yanatse [44].

Finally, we can contemplate the asymmetric form [25] for the T-matrix, so that the coupled equations for $t(Q)$ and $G(K)$ are based on

$$\chi(Q) = \sum_K G(K)G_0(Q - K) \qquad (17)$$

with self energy

$$\Sigma(K) = \sum_Q t(Q)G_0(Q - K). \qquad (18)$$

It should be noted, however, that this asymmetric form can be derived from the equations of motion by truncating the infinite series at the three-particle

level, G_3, and then factorizing the G_3 into one- and two-particle Green's functions [87]. The other two schemes are constructed diagrammatically or from a generating functional, (as apposed to derived from the Hamiltonian). *It will be made clear in what follows that, if one's goal is to extend the usual crossover ground state of Eq. (1) to finite temperatures, then one must choose the asymmetric form for the pair susceptibility, as shown in Eq. (17).* Other approaches such as the NSR approach to T_c, or that of Haussmann lead to different ground states which should, however, be very interesting in their own right . These will need to be characterized in future. Indeed, the work of Strinati group has also emphasized that the ground state associated with the T_c calculations based on NSR is distinct from that in the simple mean field theory of Eq. (1), and they presented some aspects of this comparison in Ref. 88.

Other support for this GG_0-based T-matrix scheme comes from its equivalence to self consistent Hartree-approximated Ginzburg−Landau theory [89]. Moreover, there have been detailed studies [90] to demonstrate how the superfluid density ρ_s can be computed in a fully gauge invariant (Ward Identity consistent) fashion, so that it vanishes at the self consistently determined T_c. Such studies are currently missing for the case of the other two T-matrix schemes.

Some concerns about the other two T-matrix schemes can be raised. In Ref. 24 pairing fluctuation effects are not self consistently included so that self energy corrections appear in the number equation but not in the gap equation. Similarly, the GG-based T-matrix scheme of Ref. 85 fails to recover BCS theory [87] in the weak attraction limit where pairing fluctuations are negligible.

2.3. Extending conventional crossover ground state to $T \neq 0$: T-matrix scheme in the presence of closed-channel molecules

In the T-matrix scheme we employ, the pairs are described by the pair susceptibility $\chi(Q) = = \sum_K G_0(Q - K)G(K)\varphi^2_{\mathbf{k} - \mathbf{q}/2}$ where G depends on a BCS-like self energy $\Sigma(K) \approx -\Delta^2 G_0(-K)\varphi^2_{\mathbf{k}}$. Throughout this section $\varphi_{\mathbf{k}} \equiv \exp(-k^2/2k_0^2)$ introduces a momentum cutoff, where k_0 represents the inverse range of interaction, which is assumed infinite for a contact interaction.

The noncondensed pairs [91] have propagator $t_{pg}(Q) = U_{\mathrm{eff}}(Q) / [1 + U_{\mathrm{eff}}(Q)\chi(Q)]$, where U_{eff} is the effective pairing interaction which involves the direct two-body interaction U as well as virtual excitation processes associated with the Feshbach resonance

[29,91]. At small Q, t_{pg} can be expanded, after analytical continuation $(i\Omega_n \to \Omega + i0^+)$, as

$$t_{pg}(Q) \approx \frac{Z^{-1}}{\Omega - \Omega_q + \mu_{\mathrm{pair}} + i\Gamma_Q}. \qquad (19)$$

The parameters appearing in Eq. (19) are discussed in more detail in Ref. 79. Here Z^{-1} is a residue and $\Omega_q = q^2/2M^*$ the pair dispersion, where M^* is the effective pair mass. The latter parameter as well as the pair chemical potential μ_{pair} depends on the important, but unknown, gap parameter Δ through the fermion self energy Σ. The decay width Γ_Q is negligibly small for small Q below T_c.

While there are alternative ways of deriving the self consistent equations which we use (such as a decoupling of the Green's function equations of motion [87]), here we present an approach which shows how this GG_0-based T-matrix scheme has strong analogies with the standard theory of BEC. But, importantly this BEC is embedded in a self consistent treatment of the fermions. Physically, one should focus on Δ as reflecting the presence of bosonic degrees of freedom. In the fermionic regime $(\mu > 0)$, it represents the energy required to break the pairs, so that Δ is clearly associated with the presence of «bosons». In the bosonic regime, Δ^2 directly measures the density of pairs.

In analogy with the standard theory of BEC, it is expected [91] that Δ contains contributions from both noncondensed and condensed pairs. The associated densities are proportional to $\Delta^2_{pg}(T)$ and $\tilde{\Delta}^2_{sc}(T)$, respectively. We may write the first of several constraints needed to close the set of equations. (i) One has a constraint on the *total number of pairs* [79] which can be viewed as analogous to the usual BEC number constraint

$$\Delta^2(T) \cong \Delta^2_{sc}(T) + \Delta^2_{pg}(T). \qquad (20)$$

To determine Δ, (ii) one imposes the BEC-like constraint that the pair chemical potential vanishes in the superfluid phase:

$$\mu_{\mathrm{pair}} = 0 \qquad T \leq T_c. \qquad (21)$$

This yields

$$t_{pg}^{-1}(Q \to 0) = 0 = U_{\mathrm{eff}}^{-1}(0) + \chi(0) \qquad (22)$$

so that

$$U_{\mathrm{eff}}^{-1}(0) + \sum_k \frac{1 - 2f(E_{\mathbf{k}})}{2E_{\mathbf{k}}}\varphi^2_{\mathbf{k}} = 0. \qquad (23)$$

Importantly, below T_c, Δ satisfies the usual BCS gap equation. Here we introduce the quasiparticle disper-

sion $E_{\mathbf{k}} = \sqrt{(\epsilon_{\mathbf{k}} - \mu)^2 + \Delta^2 \varphi_{\mathbf{k}}^2}$, where $\epsilon_{\mathbf{k}} = \hbar^2 k^2 / 2m$ is the fermion kinetic energy, μ is the fermionic chemical potential, and $f(x)$ is the Fermi distribution function.

(iii) In analogy with the standard derivation of BEC, the total contribution of *noncondensed* pairs is readily computed by simply adding up their number, based on the associated propagator

$$\Delta_{pg}^2 \equiv -\sum_Q t_{pg}(Q) . \tag{24}$$

One can rewrite Eq. (24) so that it looks more directly like a number equation, by introducing the Bose distribution function $b(x)$ for noncondensed pairs as

$$\Delta_{pg}^2 = Z^{-1} \sum b(\Omega_q, T), \tag{25}$$

so that the noncondensed pair density is given by $Z\Delta_{pg}^2$. Note that the right hand sides of the previous two equations depend on the unknown Δ through the self energy appearing in G which, in turn enters t_{pg} or Ω_q. Also note that at $T = 0$, $\Delta_{pg} = 0$ so that all pairs are condensed as is consistent with the mean-field BCS–Leggett ground state.

Finally, in analogy with the standard derivation of BEC, (iv) one can then compute the number of *condensed* pairs associated with $\tilde{\Delta}_{sc}$, given that one knows the total Δ and the noncondensed component.

Despite this analogy with BEC, fermions are the fundamental particles in the system. It is their chemical potential μ that is determined from the number conservation constraint

$$n = n_f + 2n_{b0} + 2n_b \equiv n_f + 2n_b^{\text{tot}}. \tag{26}$$

Here n_{b0} and n_b represent the density of condensed and noncondensed closed-channel molecules, respectively, n_b^{tot} is the sum, and $n_f = 2\sum_K G(K)$ is the atomic density associated with the open-channel fermions. These closed channel fermions have a propagator $D(Q)$, which we do not discuss in much detail in order to make the presentation simpler. Here

$$n_b = -\sum_Q D(Q) \approx Z_b \sum_q b(\Omega), \tag{27}$$

where $b(x)$ is the Bose distribution function. The renormalized propagator $D(Q)$ is given by the same equation as Eq. (19) with a different residue $Z^{-1} \to Z_b$.

In this way the system of equations is complete [91]. The numerical scheme is straightforward in principle. We compute Δ (and μ) via Eqs. (23) and (24), to determine the contribution from the condensate $\tilde{\Delta}_{sc}$ via Eqs. (20) and (24). Above T_c, this theory must be

generalized to solve self-consistently for μ_{pair} which no longer vanishes [92].

3. Physical implications: ultracold atom superfluidity

In this section we compare four distinct classes of experiments on ultracold trapped fermions with theory. These are thermodynamics [77,92], temperature dependent density profiles [93], RF pairing gap spectroscopy [72,94,95], and collective mode measurements [71,75]. We address all four experiments in the context of the mean field ground state of Eq. (1), and its finite temperature extension discussed in Section 2.3. That there appears to be good agreement between theory and experiment lends rather strong support to the simple mean field theory, which is at the center of this Review. Interestingly, pseudogap effects are evident in various ways in these experiments and this serves to tie the ultracold fermions to the high T_c superconductors.

3.1. T_c calculations and trap effects

Before turning to experiment, it is important to discuss the behavior of the transition temperature which is plotted as a function of scattering length in Fig. 10 for the homogeneous case, presuming *s*-wave pairing. We discuss the effects of *d*-wave pairing in Section 4 in the context of application to the cuprates. Starting from the BCS regime this figure shows that T_c initially increases as the interaction strength increases. However, this increase competes with the opening of a pseudogap or excitation gap $\Delta(T_c)$. Technically, the pairs become effectively heavier before they form true bound states. Eventually T_c reaches a maximum (very near unitarity) and then decreases slightly until field
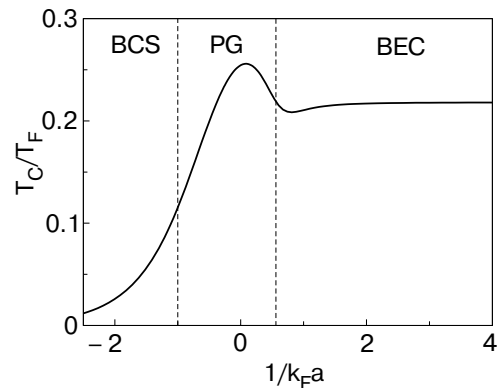
Fig. 10. Typical behavior of T_c as a function of $1/k_F a$ in a homogeneous system. T_c follows the BCS predictions and approaches the BEC asymptote $0.218 T_F$ in the BEC limit. In the intermediate regime, it reaches a maximum around $1/k_F a = 0$ and a minimum around where $\mu = 0$.

strengths corresponding to the point where μ becomes zero. At this field value (essentially where T_c is minimum), the system becomes a «bosonic» superfluid, and beyond this point T_c increases slightly to reach the asymptote corresponding to an ideal Bose gas. Somewhat different behavior in T_c appears in alternative theories where T_c is found to have a maximum near unitarity and to approach the BEC asympotote from above [24] or to have no extremal points and to approach the BEC asympote from below [85].

Trap effects change these results only quantitatively as seen in Fig. 11. However, the maximum in T_c may no longer be visible. The calculated value of T_c ($\sim 0.3 T_F$) at unitarity is in good agreement with experiment [77,96] and other theoretical estimates [97]. To treat these trap effects one introduces the local density approximation (LDA) in which T_c is computed under the presumption that the chemical potential $\mu \rightarrow \mu - V(r)$. Here we consider a spherical trap with $V(r) = 1/2(m\omega^2 r^2)$. The Fermi energy E_F is determined by the total atom number N via $E_F \equiv k_B T_F = \hbar\omega(3N)^{1/3} \equiv \hbar^2 k_F^2/2m$, where k_F is the Fermi wavevector at the center of the trap. It can be seen that the homogeneous curve is effectively multiplied by an «envelope» curve when a trap is present. This envelope, with a higher BEC asymptote, reflects the fact that the particle density at the center of the trap is higher in the bosonic, relative to the fermionic case. In this way T_c is relatively higher in the BEC regime, as compared to BCS, whenever a trap is present.

Figure 12 presents a plot of the position dependent excitation gap $\Delta(r)$ and particle density $n(r)$ profile over the extent of the trap. An important point needs to be made: because the gap is largest at the center of the trap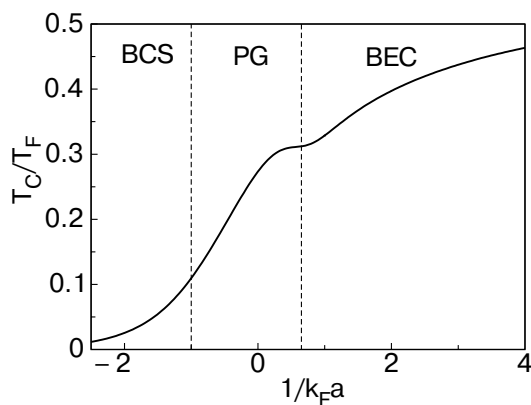, bosonic excitations will be dominant there. At the edge of the trap, by contrast, where fermions are only weakly bound (since $\Delta(r)$ is small), the excitations will be primarily fermionic. We will see the implications of these observations as we examine thermodynamic and RF spectra data in the ultracold gases.

3.2. Thermodynamical experiments

Figure 13 present a plot which compares experiment and theory in the context of thermodynamic experiments [77,92] on trapped fermions. Plotted on the vertical axis is the energy which can be input in a controlled fashion experimentally. The horizontal axis is temperature which is calibrated theoretically based on an effective temperature $\tilde{T}$ introduced phenomenologically, and discussed below. The experimental data are shown for the (effectively) non-interacting case as well as unitary. In this discussion we treat the non-interacting and BCS cases as essentially equivalent since Δ is so small on the scale of the temperatures considered. The solid curves correspond to theory for the two cases. Although not shown here, even without a temperature calibration, the data suggests a phase transition is present in the unitary case. This can be seen as a result of the change in slope of $\tilde{E}(T)$ as a function of $\tilde{T}$.

The phenomenological temperature $\tilde{T}$ is relatively easy to understand. What was done experimentally to deduce this temperature was to treat the unitary case as an essentially free Fermi gas to, thereby, infer the temperature from the width of the density profiles, but with one important proviso: a numerical constant is introduced to account for the fact that the density profiles become progressively narrower as the system varies from BCS to BEC. This systematic variation in the profile widths reflects the fact that in the free Fermi gas case, Pauli principle repulsion leads to a larger spread in the particle density than in the
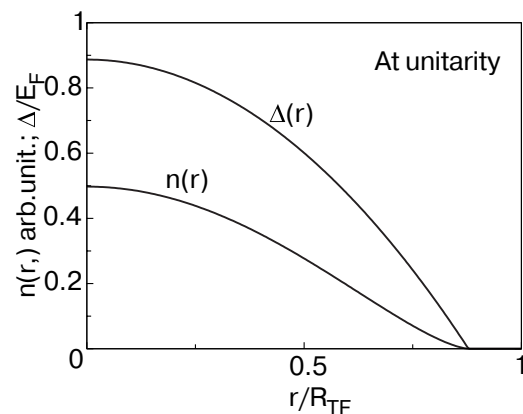

Fig. 11. Typical behavior of T_c of a Fermi gas in a trap as a function of $1/k_F a$. It follows BCS prediction in the weak coupling limit, $1/k_F a \ll -1$, and approaches the BEC asymptote $0.518 T_F$ in the limit $1/k_F a \rightarrow +\infty$. In contrast to the homogeneous case in Fig. 10, the BEC asymptote is much higher due to a compressed profile for trapped bosons.

Fig. 12. Typical spatial profile of $T = 0$ density $n(r)$ and fermionic excitation gap $\Delta(r)$ of a Fermi gas in a trap. The curves are computed at unitarity, where $1/k_F a = 0$. Here R_{TF} is the Thomas−Fermi radius.
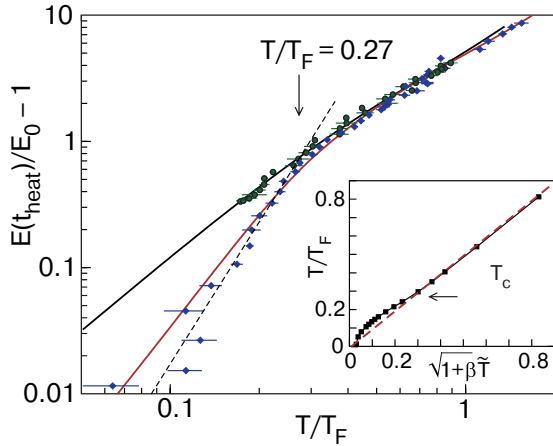
Fig. 13. Energy E vs physical temperature T. The upper curve and data points correspond to the BCS or essentially free Fermi gas case, and the lower curve and data correspond to unitarity. The latter provide indications for a phase transition. The inset shows how temperature must be recalibrated below T_c. From Ref. 77.

bosonic case. And the unitary regime has a profile width which is somewhere in between, so that one parametrizes this width by a simple function of β. We can think of β as reflecting bosonic degrees of freedom, within an otherwise fermionic system. At $\beta \equiv 0$ the system is a free Fermi gas. The principle underlying this rescaling of the non-interacting gas is known as the «universality hypothesis» [96,98]. At unitarity, the Fermi energy of the non-interacting system is the only energy scale in the problem (for the widely used contact potential) since all other scales associated with the two-body potential drop out when $a_s \to \pm \infty$. We refer to this phenomenological fitting temperature procedure as Thomas–Fermi (TF) fits.

An interesting challenge was to relate this phenomenological temperature $\tilde{T}$ to the physical temperature T; more precisely one compares $\sqrt{1 + \beta}\,\tilde{T}$ and T. This relationship is demonstrated in the inset of Fig. 13. And it was in this way that the theory and experiment could be plotted on the same figure, as shown in the main body of Fig. 13. The inset was obtained using theory only. The theoretically produced profiles were analyzed just as the experimental ones to extract $\sqrt{1 + \beta}\,\tilde{T}$ and compare it to the actual T. Above T_c no recalibration was needed as shown by the straight line going through the diagonal. Below T_c the phenomenologically deduced temperatures were consistently lower than the physical temperature. That the normal state temperatures needed no adjustment shows that the phenomenology captures important physics. It

misses, however, an effect associated with the presence of a condensate which we will discuss shortly.

We next turn to a more detailed comparison of theory and experiment for the global and low T thermodynamics. Figure 14 presents a blow-up of E at the lowest T comparing the unitary and non-interacting regimes. The agreement between theory and experiment is quite good. In the figure, the temperature dependence of E reflects primarily fermionic excitations at the edge of the trap, although there is a small bosonic contribution as well. It should be noted that the theoretical plots were based on fitting β to experiment by picking a magnetic field very slightly off resonance. (In the simple mean field theory $\beta = -0.41$, and in Monte Carlo simulations [60] $\beta = -0.54$. Both these theoretical numbers lie on either side of experiment [77] where $\beta = -0.49$).

Figure 15 presents a wider temperature scale plot which, again, shows very good agreement. Importantly one can see the effect of a pseudogap in the unitary case. The temperature T^* can be picked out from the plots as that at which the non-interacting and unitary curves intersect. This corresponds roughly to $T^* \approx 2T_c$.

3.3. Temperature dependent particle density profiles

In order to understand more deeply the behavior of the thermodynamics, we turn next to a comparison of finite T density profiles. Experiments which measure these profiles [74,99] all report that they are quite smooth at unitarity, without any signs of the bimodality seen in the BEC regime. We discuss these profiles in terms of the four panels in Fig. 16. These fig-
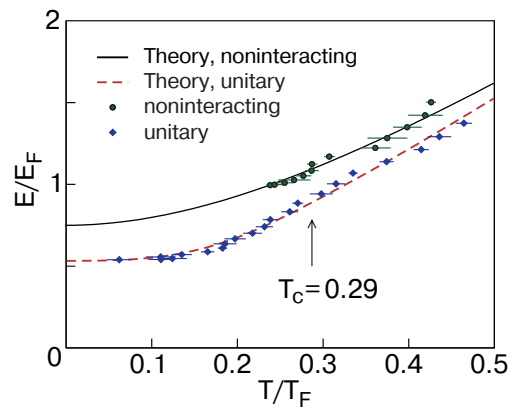

Fig. 14. Low temperature comparison of theory (curves) and experiments (symbols) in terms of E/E_F ($E_F = k_B T_F$) per atom as a function of T/T_F, for both unitary and noninteracting gases in a Gaussian trap. From Ref. 77.
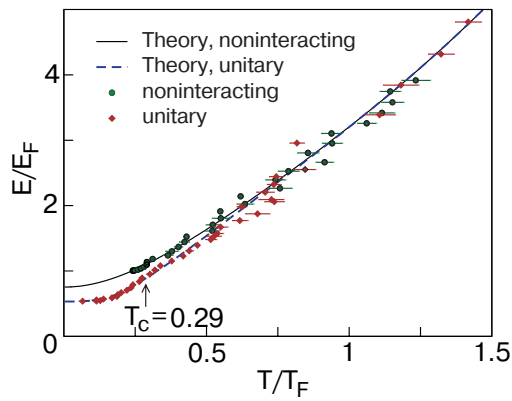
Fig. 15. Same as Fig. 14 but for a much larger range of temperature. The quantitative agreement between theory and experiment is very good. The fact that the two experimental (and the two theoretical) curves do not merge until higher $T^* > T_c$ is consistent with the presence of a pseudogap.

ures are a first step in understanding the previous temperature calibration procedure.

In this figure we compare theory and experiment for the unitary case. The experimental data were estimated to correspond to roughly this same temperature $(T/T_F = 0.19)$ based on the calibration procedure discussed above. The profiles shown are well within the superfluid phase $(T_c \approx 0.3 T_F$ at unitarity). This figure presents Thomas–Fermi fits [99] to (a) the experimental and (b) theoretical profiles as well as (c) their comparison, for a chosen $R_{TF} = 100$ μm, which makes it possible to overlay the experimental data (circles) and theoretical curve (line). Finally Fig. 16,d indicates the relative χ^2 or root-mean-square (rms) deviations for these TF fits to theory. This figure was made in collaboration with the authors of Ref. 99. Two of the three-dimensions of the theoretical trap profiles were integrated out to obtain a one-dimensional representation of the density distribution along the transverse direction: $\bar{n}(x) \equiv \int dy\,dz\, n(r)$.

This figure is in contrast to earlier theoretical studies which predict a significant kink at the condensate edge which appears not to have been seen experimentally [74,99]. Moreover, the curves behave monotonically with both temperature and radius. Indeed, in the unitary regime the generalized TF fitting procedure of Ref. 99 works surprisingly well. And these reasonable TF fits apply to essentially all temperatures investigated experimentally [99], as well as theoretically, including in the normal state.

It is important to establish why the profiles are so smooth, and the condensate is, in some sense, rather invisible, except for its effect on the TF-inferred-temperature. This apparent smoothness can be traced to the presence of noncondensed pairs of fermions which need
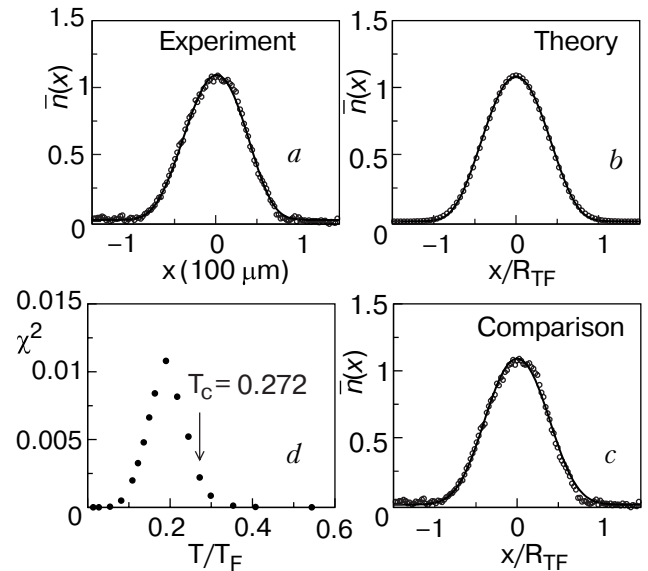

Fig. 16. Temperature dependence of (a) experimental one-dimensional spatial profiles (circles) and TF fit (line) from Ref. 99, (b) TF fits (line) to theory both at $T \approx 0.7 T_c \approx 0.19 T_F$ (circles) and (c) overlay of experimental (circles) and theoretical (line) profiles, as well as (d) relative rms deviations (χ^2) associated with these fits to theory at unitarity. The circles in (b) are shown as the line in (c). The profiles have been normalized so that $N = \int \bar{n}(x)\,dx = 1$, and we set $R_{TF} = 100$ μm in order to overlay the two curves. χ^2 reaches a maximum around $T = 0.19 T_F$.

to be included in any consistent treatment. Indeed, these pairs below T_c are a natural counterpart of the pairs above T_c which give rise to pseudogap effects.

To see how the various contributions enter into the trap profile, in Fig. 17 we plot a decomposition of this profile for various temperatures from below to above T_c. The various color codes indicate the condensate along with the noncondensed pairs and the fermions. This decomposition is based on the superfluid density so that all atoms participate in the condensation at $T = 0$. This, then, forms the basis for addressing both thermodynamics and RF pairing-gap spectroscopy in this Review.

The figure shows that by $T = T_c/2$ there is a reasonable number of excited fermions and bosons. As anticipated earlier in Section 2.3, the latter are at the trap edge and the former in the center. By $T = T_c$ the condensate has disappeared and the excitations are a mix of fermions (at the edge) and bosons towards the center. Indeed, the noncondensed bosons are still present by $T = 1.5 T_c$, as a manifestation of a pseudogap effect. Only for somewhat higher $T \approx 2 T_c$ do they disappear
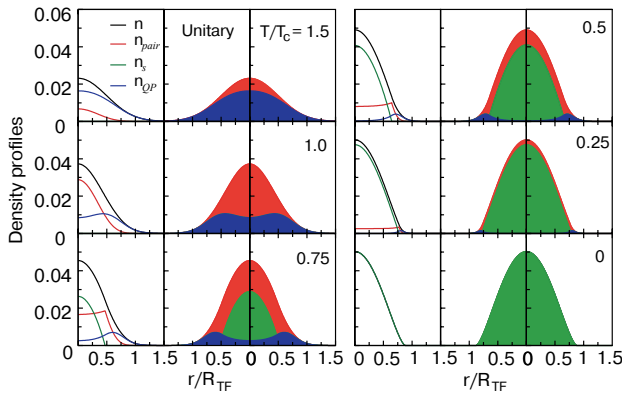
Fig. 17. Decomposition of density profiles at various temperatures at unitarity. Here (light gray) refers to the condensate, (dark gray) to the noncondensed pairs and (black) to the excited fermionic states. $T_c = 0.27 T_F$, and R_{TF} is the Thomas–Fermi radius.

altogether, so that the system becomes a non-interacting Fermi gas.

Two important points should be made. The noncondensed pairs clearly are responsible for smoothing out what otherwise would be a discontinuity [98,100] between the fermionic and condensate contributions. Moreover, the condensate shrinks to the center of the trap as T is progressively raised. It is this thermal effect which is responsible for the fact that the TF fitting procedure for extracting temperature leads to an underestimate as shown in the inset to Fig. 13. The presence of the condensate tends to make the atomic cloud smaller so that the temperature appears to be lower in the TF fits.

3.4. RF pairing gap spectroscopy

Measurements [72] of the excitation gap Δ have been made by using a third atomic level, called $|3\rangle$, which does not participate in the superfluid pairing. Under application of RF fields, one component of the Cooper pairs, called $|2\rangle$, is presumably excited to state $|3\rangle$. If there is no gap Δ then the energy it takes to excite $|2\rangle$ to $|3\rangle$ is the atomic level splitting ω_{23}. In the presence of pairing (either above or below T_c) an extra energy Δ must be input to excite the state $|2\rangle$, as a result of the breaking of the pairs. Figure 18 shows a plot of the spectra near unitarity for four different temperatures, which we discuss in more detail below. In general for this case, as well as for the BCS and BEC limits, there are two peak structures which appear in the data: the sharp peak at $\omega_{23} \equiv 0$ which is associated with «free» fermions at the trap edge and the broader peak which reflects the presence of paired atoms; more directly this broad peak derives from the distribution of Δ in the trap. At high T (compared to

Δ), only the sharp feature is present, whereas at low T only the broad feature remains. The sharpness of the free atom peak can be understood as coming from a large phase space contribution associated with the $2 \rightarrow 3$ excitations [95]. Clearly, these data alone do not directly indicate the presence of superfluidity, but rather they provide strong evidence for pairing.

As pointed out in Ref. 94 these experiments serve as a counterpart to superconducting tunneling in providing information about the excitation gap. A theoretical understanding of these data was first presented in Ref. 76 using the framework of Section 2.3. Subsequent work [95] addressed these data in a more quantitative fashion as plotted in Fig. 19. Here the upper and lower panels correspond respectively to intermediate and low temperatures. For the latter one sees that the sharp «free atom» peak has disappeared, so that fermions at the edge of the trap are effectively bound at these low T. Agreement between theory and experiment is quite satisfactory, although the total
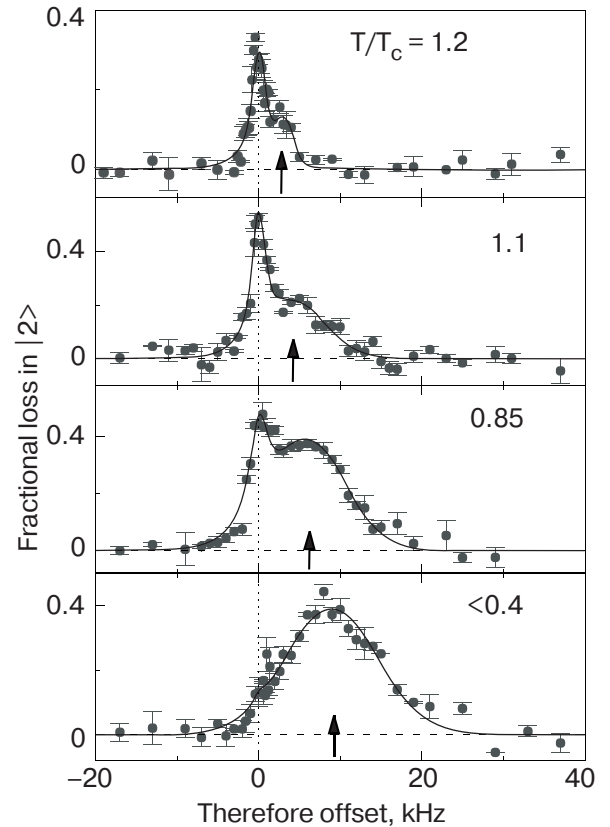

Fig. 18. Experimental RF spectra at unitarity. The temperatures labeled in the figure were computed theoretically at unitarity based on adiabatic sweeps from BEC. The two top curves, thus, correspond to the normal phase, thereby, indicating pseudogap effects. Here $E_F = 2.5$ μK, or 52 kHz. From Ref. 72.

number of particles was adjusted somewhat relative to the experimental estimates.

It is interesting to return to the previous figure (Fig. 18) and to discuss the temperatures in the various panels. What is measured experimentally are temperatures T' which correspond to the temperature at the start of a sweep from the BEC limit to unitarity. Here fits to the BEC-like profiles are used to deduce T' from the shape of the Gaussian tails in the trap. Based on knowledge about thermodynamics (entropy S), and given T', one can then compute the final temperature in the unitary regime, assuming S is constant. Indeed, this adiabaticity has been confirmed experimentally in related work [74]. We find that the four temperatures are as indicated in the figures. Importantly, one can conclude that the first two cases correspond to a normal state, albeit close to T_c. Importantly, these figures suggest that a pseudogap is present as reflected by the broad shoulder above the narrow free atom peak.

3.5. Collective breathing modes at $T \approx 0$

We turn, finally, to a comparison between theory [101,102] and experiment [71,75,96,103] for the collective breathing modes within a trap at $T \approx 0$. The very good agreement has provided some of the earliest and strongest support for the simple mean field theory of Eq. (1). Interestingly, Monte Carlo simulations which initially were viewed as a superior approach,
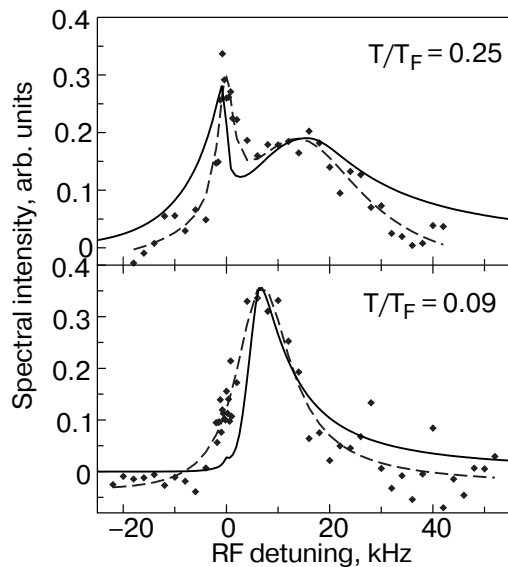
lead to significant disagreement between theory and experiment [104]. Shown in Fig. 20 is this comparison for the axial mode in the inset and the radial mode in the main body of the figure as a function of magnetic field. The experimental data are from Ref. 71. The original data on the radial modes from Ref. 75, was in disagreement with that of Ref. 71, but this has since been corrected [104], and there is now a consistent experimental picture from both the Duke and the Innsbruck groups for the radial mode frequencies.

At $T = 0$, calculations of the mode frequencies can be reduced to a calculation of an equation of state for μ as a function of n. One of the most important conclusions from this figure is that the behavior in the near-BEC limit (which is still far from the BEC asymptote) shows that the mode frequencies *decrease* with increasing magnetic field. This is opposite to earlier predictions [105] based on the behavior of true bosons where a Lee-Yang term would lead to an increase. Indeed, the pair operators do not obey the commutation relations of true bosons except in the zero density or $k_F a \rightarrow 0^+$ limit [106]. Figure 20, thus, underlines the fact that fermionic degrees of freedom (or compositeness) are still playing a role at these magnetic fields. There are predictions in the literature [107] that one needs to achieve $k_F a$ somewhat less than 0.3 (experimentally, the smallest values for these experiments are 0.3 and 0.7 for the various groups) in order to approach the true bosonic limit. At this point, then, the simple mean field theory will no longer be
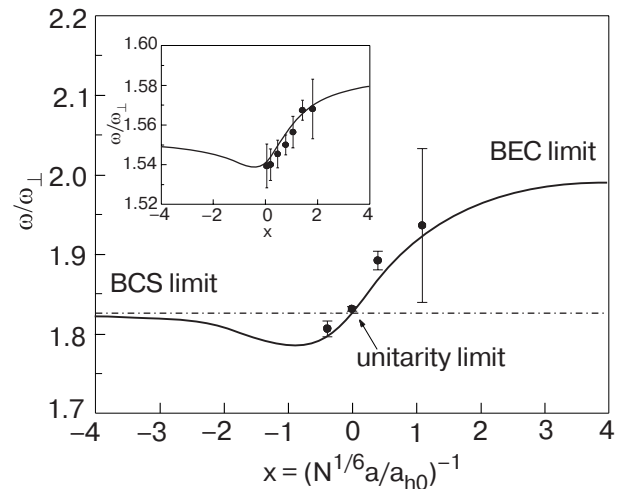

Fig. 19. Comparison of calculated RF spectra (solid curve, $T_c \approx 0.29\,T_F$) with experiment (symbols) in a harmonic trap calculated at 822 G for the two lower temperatures. The temperatures were chosen based on Ref. 72. The particle number was reduced by a factor of 2, as found to be necessary in addressing another class of experiments [88]. The dashed lines are a guide to the eye. From Ref. 95.

Fig. 20. Breathing mode frequencies as a function of $\kappa \approx 1.695(k_F a)^{-1}$, from Tosi et al. [10]. The main figure and inset plot the transverse and axial frequencies, respectively. The solid curves are calculations [101] based on BCS−BEC crossover theory at $T = 0$, and the symbols plot the experimental data from Kinast et al. [71]. Here N is total atom number, and a_{ho} the harmonical oscillator length.

adequate. Indeed, there are other indications [108] of the breakdown of this mean field in the extreme BEC limit which are, physically, reflected in the width of the particle density profiles. This originates from an overestimate (by roughly a factor of 3) of the size of the effective «inter-boson» scattering length.

Overall the mean field theory presented here looks very promising. Indeed, the agreement between theory and experiment is better than one might have anticipated. For the collective mode frequencies, it appears to be better than Monte Carlo calculations [104]. Nevertheless, uncertainties remain. Theories which posit a different ground state will need to be compared with the four experiments discussed here. It is, finally, quite possible that incomplete $T = 0$ condensation will become evident in future experiments. If so, an alternative wavefunction will have to be contemplated [107,109]. What appears to be clear from the current experiments is that, just as in high T_c superconductors, the ultracold fermionic superfluids exhibit pseudogap effects. These are seen in thermodynamics, in RF spectra and in the temperature dependence of the profiles (through the noncondensed pair contributions). Moreover, while not discussed here, at finite T, damping of the collective mode frequencies seems to change qualitatively [96] at a temperature which is close to the estimated T^*.

Looking to the future, at an experimental level, new pairing gap spectroscopies appear to be emerging at a fairly rapid pace [110,111]. These will further test the present and subsequent theories. Indeed, recently, a probe of the closed channel overtion [111] has been analyzed [112] within the present framework and has led to good quantitative agreement between theory and experiment.

4. Physical implications: high T_c superconductivity

4.1. Phase diagram and superconducting coherence

The high T_c superconductors are different from the ultracold fermionic superfluids in one key respect; they are d-wave superconductors and their electronic dispersion is associated with a quasi-two dimensional tight binding lattice. In many ways this is not a profound difference from the perspective of BCS−BEC crossover. Figure 21 shows a plot of the two important temperatures T_c and T^* as a function of increasing attractive coupling. On the left is BCS and the right is PG. The BEC regime is not visible. This is because T_c disappears before it can be accessed. This disappearance of T_c is relatively easy to understand. Because the d-wave pairs are more extended (than their s-wave counterparts) they experience Pauli principle repul-

sion more intensely. Consequently the pairs localize (their mass is infinite) well before the fermionic chemical potential is negative [42].

The competition between T^* and T_c, in which as T^* increases, T_c decreases, is also apparent in Fig. 21. This is a consequence of pseudogap effects. More specifically, the pairs become heavier as the gap increases in the fermionic spectrum, competing with the increase of T_c due to the increasing pairing strength. It is interesting to compare Fig. 21 with the experimental phase diagram plotted as a function of the doping concentration x in Fig. 5. If one inverts the horizontal axis (and ignores the unimportant AFM region) the two are very similar. To make an association from coupling U to the variable x, it is reasonable to fit T^*. It is not particularly useful to implement this last step here, since we wish to emphasize crossover effects which are not complicated by «Mott physics».

Because of quasi-two dimensionality, the energy scales of the vertical axis in Fig. 21 are considerably smaller than their three-dimensional analogues. Thus, pseudogap effects are intensified, just as conventional fluctuation effects are more apparent in low-dimensional systems. This may be one of the reasons why the cuprates are among the first materials to clearly reveal pseudogap physics. Moreover, the present calculations show that in a strictly 2D material, T_c is driven to zero, by bosonic or fluctuation effects. This is a direct reflection of the fact that there is no Bose condensation in 2D.

The presence of pseudogap effects raises an interesting set of issues surrounding the signatures of the transition which the high T_c community has wrestled with, much as the cold atom community is doing today. For a charged superconductor there is no difficulty in measuring the superfluid density, through the
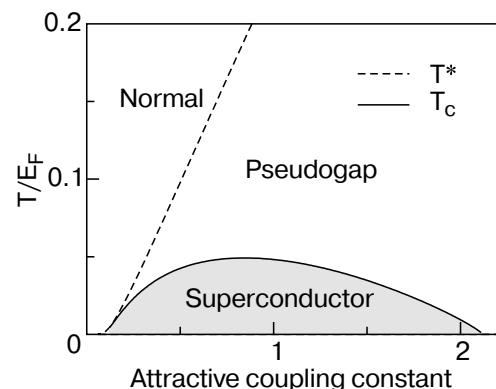

Fig. 21. Typical phase diagram for a quasi-two dimensional d-wave superconductor on a tight-binding lattice at high filling $n \approx 0.85$ per unit cell; here the horizontal axis corresponds to $-U/4t$, where t is the in-plane hopping matrix element.

electrodynamic response. Thus one knows with certainty where T_c is. Nevertheless, people have been concerned about precisely how the onset of phase coherence is reflected in thermodynamics, such as C_v or in the fermionic spectral function, given that a gap is already present at the onset of superconductivity. One understands how phase coherence shows up in BCS theory, since the ordered state is always accompanied by the appearance of an excitation gap.

To address these coherence effects one has to introduce a distinction [115] between the self energy associated with noncondensed and condensed pairs. This distinction is blurred by the approximations made in Section 2.3. Within this improved scheme [115] superconducting coherence effects can be probed as, presented in Fig. 22, along with a comparison to experiment. Shown are the results of specific heat and tunneling calculations and their experimental counterparts [2,33]. The latter measures, effectively, the density of fermionic states. Here the label «PG» corresponds to an extrapolated normal state in which we set the superconducting order parameter Δ_{sc} to zero, but maintain the the total excitation gap Δ to be the same as in a phase coherent, superconducting state. Agreement between theory and experiment is satisfactory.

4.2. Electrodynamics in the superconducting phase

In some ways the subtleties of phase coherent pairing are even more perplexing in the context of electrodynamics. Figure 7 presents a paradox in which the excitation gap for fermions appears to have little to do with the behavior of the superfluid density. This superfluid density can be readily computed within the BCS−BEC crossover scenario [25,48]. Particularly important is to include all excitations of the condensate in a fully consistent fashion, compatible with thermodynamics, and which is also manifestly gauge invariant. To make contact with electrodynamic experiments, one has to introduce the variable x and this is done via a fit to $T^*(x)$ in the phase diagram. In addition it is also necessary to fit $\rho_s(T=0, x)$ to experiment, and we do so here, noting that [32] the Uemura relation $\rho_s(0, x) \propto T_c(x)$ no longer holds for very underdoped samples [114,116]. By fitting these x-dependent quantities we are, in effect accounting for at least some aspects of Mott physics. The paradox raised by Fig. 7 is resolved by noting that there are bosonic excitations of the condensate [25] and that these become more marked with underdoping, as pseudogap effects increase. In this way ρ_s does not exclusively reflect the fermionic gap, but rather vanishes «prematurely» before this gap is zero, as a result of pair excitations of the condensate.
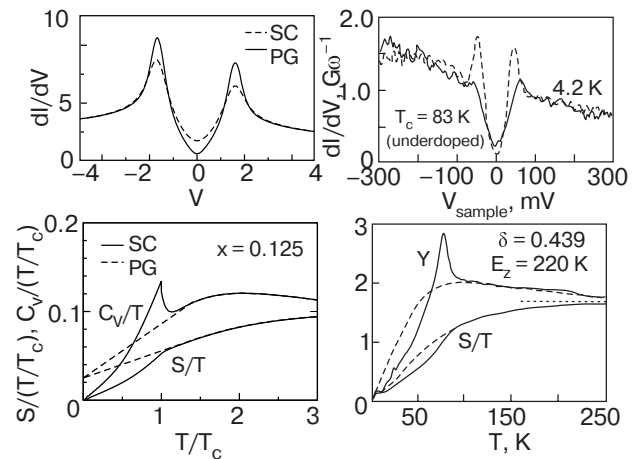

Fig. 22. Extrapolated normal state (PG) and superconducting state (SC) contributions to SIN tunneling and thermodynamics (left), as well as comparison with experiments (right) on tunneling for BSCCO [33] and on specific heat for $Y_{0.8}Ca_{0.2}Ba_2Cu_3O_{7-\delta}$ [113]. The theoretical SIN curve is calculated for $T = T_c/2$, while the experimental curves are measured outside (dashed line) and inside (solid line) a vortex core.

This theory can be quantitatively compared with experiment. Figure 23 presents theoretical and experimental plots of the lower critical field, $H_{c1}(T)$, for a group of severely underdoped YBCO crystals as considered in Ref. 114. There it was argued that $H_{c1}(T) \propto \rho_s(T)$, so that the lower critical field effectively measures the in-plane superfluid density. Experimentally what is directly measured is the magnetization with applied field parallel to the c-axis. The experimental results are shown on the lower two panels and theory on the upper two. The left hand figures plot $H_{c1}(T)$ vs T and the right hand figures correspond to a rescaling of this function in the form $H_{c1}(T)/H_{c1}(0)$ vs T/T_c. Theoretically, it is found that the fermionic contribution leads to a linear T dependence at low T, associated with d-wave pairing, whereas the bosonic term introduces a $T^{3/2}$ term. Quite remarkably even when the Uemura relation no longer holds, there is still a «universality» in the normalized plots as shown in both theory and experiment by the right hand figures. It should be noted that the experimental plot contains (at $T_c = 55.5\,K$) a slightly different cuprate phase known as the ortho-II phase, which does not lie on the universal curves. The universality found here can be understood as associated with the fact that $T_c(x)$, rather than $\Delta(x)$, is the fundamental energy scale in $\rho_s(T, x)$. The reason that $\Delta(x)$ is not the sole energy scale is that bosonic degrees of freedom are also present, and help to drive ρ_s to zero at T_c. By contrast, Fermi-liquid based approaches [114,117] assume that the fermions are the only rele-
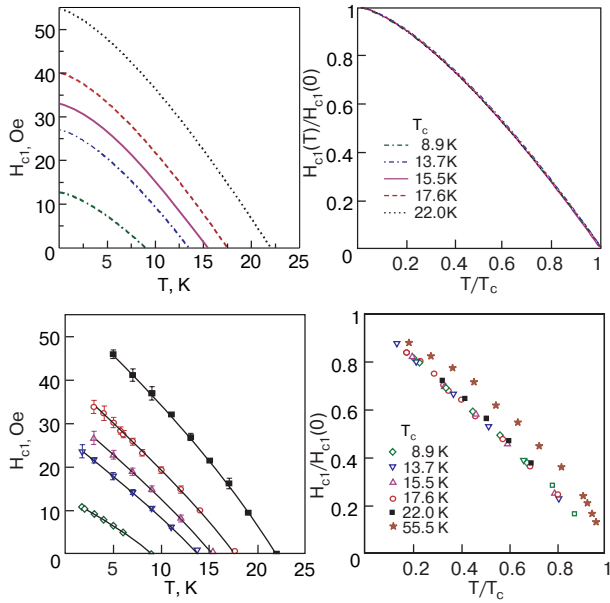
Fig. 23. Comparison between calculated lower critical field, H_{c1}, as a function of T (upper left panel), and experimental data (lower left) from Ref. 114, with variable doping concentration x. The right column shows normalized plots, $H_{c1}(T)/H_{c1}(0)$ versus T/T_c, for theory and experiment, respectively, revealing a quasi-universal behavior with respect to doping, with the exception of the $T_c = 55.5$ K ortho-II phase. Both theory plots share the same legends. The quantitative agreement between theory and experiment is quite good.

vant excitations, and they account for this data by introducing a phenomenological parameter α which corresponds to the effective charge of the fermionic quasi-particles.

As anticipated in earlier theoretical calculations [25] the bosonic contribution begins to dominate in severely underdoped systems so that the slope dH_{c1}/dT (associated with the lowest temperatures reached experimentally) should *decrease* with underdoping. Although observed a number of years after this prediction, this is precisely what is seen experimentally, as shown in Fig. 24. Here the inset plots the experimental counterpart data. It can be seen that theory and experiment are in reasonably good quantitative agreement. This theoretical viewpoint is very different from a «Fermi-liquid» based treatment of the superconducting state, for which the strong decrease in the slope of H_{c1} was not expected. Within the present formalism, the optical conductivity [1] $\sigma(\omega)$ is similarly modified [118] to include bosonic as well as fermionic contributions.

4.3. Bosonic power laws and pairbreaking effects

The existence of noncondensed pair states below T_c affects thermodynamics, in the same way that electro-
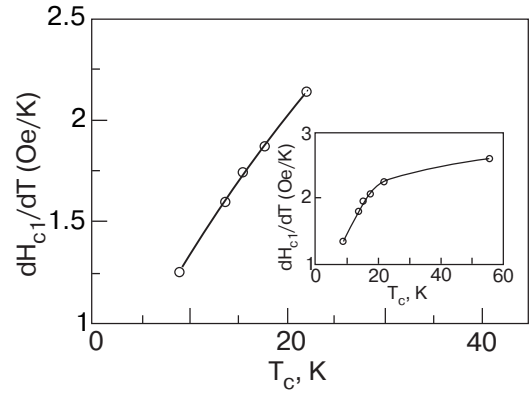

Fig. 24. Comparison of theoretically calculated low T slope dH_{c1}/dT (main figure) for various doping concentrations (corresponding to different T_c) in the underdoped regime with experimental data (inset) from Ref. 114. The theoretical slopes are estimated using the low temperature data points accessed experimentally. The quantitative agreement is very good.

dynamics is affected, as discussed above. Moreover, one can predict [36] that the q^2 dispersion will lead to ideal Bose gas power laws in thermodynamical and transport properties. These will be present in addition to the usual power laws or (for *s*-wave) exponential temperature dependencies associated with the fermionic quasiparticles. Note that the q^2 dependence is dictated by the ground state of Eq. (1). Clearly this mean field like state is inapplicable in the extreme BEC limit, where, presumably interboson effects become important and lead to a linear dispersion. Presumably, in the PG or near-BEC regimes, fermionic degrees of freedom are still dominant and it is reasonable to apply Eq. (1). Importantly, at present neither the cuprates nor the cold atom systems access this true BEC regime.

The consequences of these observations can now be listed [36]. For a quasi-two dimensional system, C_v/T will appear roughly constant at the lowest temperatures, although it vanishes strictly at $T = 0$ as $T^{1/2}$. The superfluid density $\rho_s(T)$ will acquire a $T^{3/2}$ contribution in addition to the usual fermionic terms. By contrast, for spin singlet states, there is no explicit pair contribution to the Knight shift. In this way the low T Knight shift reflects only the fermions and exhibits a scaling with $T/\Delta(0)$ at low temperatures. Experimentally, in the cuprates, one usually sees a finite low T contribution to C_v/T. A Knight shift scaling is seen. Finally, also observed is a deviation from the predicted *d*-wave linear in T power law in ρ_s. The new power laws in C_v and ρ_s are conventionally attributed to impurity effects. Experiments are not yet at a stage to clearly distinguish between these two alternative explanations.

Pairbreaking effects are viewed as providing important insight into the origin of the cuprate pseudogap. Indeed, the different pairbreaking sensitivities of T^* and T_c are usually proposed to support the notion that the pseudogap has nothing to do with superconductivity. To counter this incorrect inference, a detailed set of studies was conducted (based on the BEC−BCS scenario), of pairbreaking in the presence of impurities [119,120] and of magnetic fields [121]. These studies make it clear that the superconducting coherence temperature T_c is far more sensitive to pairbreaking than is the pseudogap onset temperature T^*. Indeed, the phase diagram of Fig. 21 which mirrors its experimental counterpart, shows the very different, even competing nature of T^* and T_c, despite the fact that both arise from the same pairing correlations.

4.4. Anomalous normal state transport: Nernst coefficient

Much attention is given to the anomalous behavior of the Nernst coefficient in the cuprates [49]. This coefficient is rather simply related to the transverse thermoelectric coefficient α_{xy} which is plotted in Fig. 25. In large part, the origin of the excitement in the literature stems from the fact that the Nernst coefficient behaves smoothly through the superconducting transition. Below T_c it is understood to be associated with superconducting vortices. Above T_c if the system were a Fermi liquid, there are arguments to prove that the Nernst coefficient should be essentially zero. Hence the observation of a non-negligible Nernst contribution has led to the picture of fluctuating «normal state vortices».

The formalism of Ref. 51 can be used to address these data within the framework of BCS−BEC crossover. The results are plotted in Fig. 25 with a subset of the data plotted in the upper right inset. It can be seen that the agreement is reasonable. In this way a «pre-formed pair» picture appears to be a viable alternative to «normal state vortices». It will, ultimately, be necessary to take these transport calculations below T_c. This is a project for future research and in this context it will be important to establish in this picture how superconducting state vortices are affected by the noncondensed pairs and conversely.

5. Conclusions

In this Review we have summarized a large body of work on the subject of the BCS−BEC crossover scenario. In this context, we explored the intersection of two very different fields: high T_c superconductivity and cold atom superfluidity. Theories of cuprate superconductivity can be crudely classified as focusing on «Mott physics» which reflects the anomalously
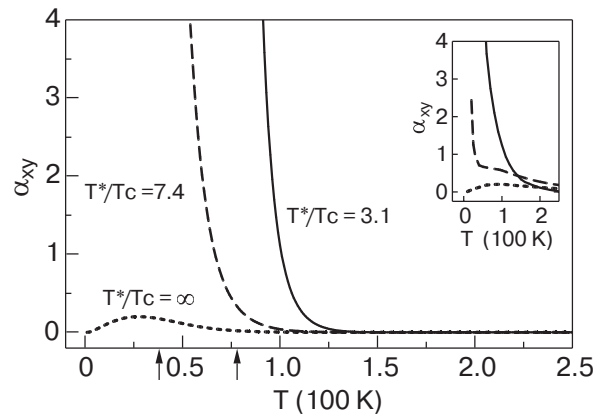

Fig. 25. Calculated transverse thermoelectric response, which appears in the Nernst coefficient, as a function of temperature for the underdoped cuprates.

small zero temperature superfluid density and «crossover physics», which reflects the anomalously short coherence length. Both schools are currently very interested in explaining the origin of the mysterious pseudogap phase. In this Review we have presented a case for its origin in crossover physics. The pseudogap in the normal state can be associated with metastable pairs of fermions; a (pseudogap) energy must be supplied to break these pairs apart into their separate components. The pseudogap also persists below T_c in the sense that there are noncondensed fermion pair excitations of the condensate.

The recent discovery of superfluidity in cold fermion gases opens the door to a set of fascinating problems in condensed matter physics. Unlike the bosonic system, there is no counterpart of Gross−Pitaevskii theory. A new theory which goes beyond BCS and encompasses BEC in some form or another will have to be developed in concert with experiment. *As of this writing, there are four experiments where the simple mean field theory discussed in this review is in reasonable agreement with the data.* These include the collective mode studies over the entire range of accessible magnetic fields [101,102]. In addition in the unitary regime, RF spectroscopy-based pairing gap studies [76,95], as well as density profile [93] and thermodynamic studies [77,92] all appear to be compatible with this theory. Interestingly, all of these provide indications for a pseudogap either directly through the observation of the normal state energy scales, T^* and Δ, or indirectly, through the observation of noncondensed pairs. The material in this Review is viewed as the first of many steps in a long process. It is intended to provide continuity from one community (which has addressed the BCS−BEC crossover scenario, since the early 1990's) to another.

1. T. Timusk and B. Statt, *Rep. Prog. Phys.* **62**, 61 (1999).

2. J.L. Tallon and J.W. Loram, *Physica* **C349**, 53 (2001).

3. H. Ding, T. Yokoya, J.C. Campuzano, T. Takahashi, M. Randeria, M.M.R. Norman, T. Mochiku, K. Hadowaki, and J. Giapintzakis, *Nature* **382**, 51 (1996).

4. R. Damascelli, Z. Hussain, and Z.-X. Shen, *Rev. Mod. Phys.* **75**, 473 (2003).

5. S.W. Cheong, G. Aeppli, T.E. Mason, H.A. Mook, S.M. Hayden, P.C. Canfield, Z. Fisk, K.N. Clausen, and J.L. Martinez, *Phys. Rev. Lett.* **67**, 1791 (1991).

6. H.F. Fong, B. Keimer, P.W. Anderson, D. Reznik, F. Dogan, and I.A. Aksay, *Phys. Rev. Lett.* **75**, 316 (1995).

7. M.A. Kastner, R.J. Birgeneau, G. Shirane, and Y. Endoh, *Rev. Mod. Phys.* **70**, 897 (1998).

8. G. Aeppli, T.E. Mason, S.M. Hayden, H.A. Mook, and J. Kulda, *Science* **278**, 1432 (1997).

9. G. Aeppli, T.E. Mason, H.A. Mook, A. Schroeder, and S.M. Hayden, *Physica* **C282−287**, 231 (1997).

10. H.A. Mook, P. Dai, S.M. Hayden, G. Aeppli, T.G. Perring, and F. Dogan, *Nature* **395**, 580 (1998).

11. J. Rossat-Mignod, L.P. Regnault, C. Vettier, P. Bourges, P. Burlet, J. Bossy, J.Y. Henry, and G. Lapertot, *Physica* **C185**, 86 (1991).

12. J.M. Tranquada, P.M. Gehring, G. Shirane, S. Shamoto, and M. Sato, *Phys. Rev.* **B46**, 5561 (1992).

13. D.A. Wollman, D.J. Van Harlingen, J. Giapintzakis, and D.M. Ginsberg, *Phys. Rev. Lett.* **74**, 797 (1995).

14. C.C. Tsuei, J.R. Kirtley, C.C. Chi, L.S. Yu-Jahnes, A. Gupta, T. Shaw, J.Z. Sun, and M.B. Ketchen, *Phys. Rev. Lett.* **73**, 593 (1994).

15. A. Mathai, Y. Gim, R.C. Black, A. Amar, and F.C. Wellstood, *Phys. Rev. Lett.* **74**, 4523 (1995).

16. To be precise, the gap and pseudogap do not contain a phase and thus have $|d_{x^2-y^2}|$ symmetry, while the order parameter has $d_{x^2-y^2}$ symmetry.

17. M. Holland, S.J.J.M.F. Kokkelmans, M.L. Chiofalo, and R. Walser, *Phys. Rev. Lett.* **87**, 120406 (2001).

18. E. Timmermans, K. Furuya, P.W. Milonni, and A.K. Kerman, *Phys. Lett.* **A285**, 228 (2001).

19. D.M. Eagles, *Phys. Rev.* **186**, 456 (1969).

20. A.J. Leggett, in: *Modern Trends in the Theory of Condensed Matter*, Springer-Verlag, Berlin (1980), p. 13.

21. R. Micnas, J. Ranninger, and S. Robaszkiewicz, *Rev. Mod. Phys.* **62**, 113 (1990).

22. M. Randeria, in: *Bose-Einstein Condensation*, A. Griffin, D. Snoke, and S. Stringari (eds.), Cambridge Univ. Press, Cambridge (1995), p. 355.

23. R. Cote and A. Griffin, *Phys. Rev.* **B48**, 10404 (1993).

24. P. Noziéres and S. Schmitt-Rink, *J. Low Temp. Phys.* **59**, 195 (1985).

25. Q.J. Chen, I. Kosztin, B. Jankó, and K. Levin, *Phys. Rev. Lett.* **81**, 4708 (1998).

26. R. Micnas and S. Robaszkiewicz, *Cond. Matt. Phys.* **1**, 89 (1998).

27. J. Ranninger and J.M. Robin, *Phys. Rev.* **B53**, R11961 (1996).

28. J.N. Milstein, S.J.J.M.F. Kokkelmans, and M.J. Holland, *Phys. Rev.* **A66**, 043604 (2002).

29. Y. Ohashi and A. Griffin, *Phys. Rev. Lett.* **89**, 130402 (2002).

30. A. Griffin and Y. Ohashi, *Phys. Rev.* **A67**, 063612 (2003).

31. P. Pieri, L. Pisani, and G.C. Strinati, *Phys. Rev. Lett.* **92**, 110401 (2004).

32. Y.J. Uemura, *Physica* **C282−287**, 194 (1997).

33. Ch. Renner, B. Revaz, K. Kadowaki, I. Maggio-Aprile, and O Fischer, *Phys. Rev. Lett.* **80**, 3606 (1998).

34. G. Deutscher, **Nature 397**, 410 (1999).

35. A. Junod, A. Erb, and Ch. Renner, *Physica* **C317−318**, 333 (1999).

36. Q.J. Chen, I. Kosztin, and K. Levin, *Phys. Rev. Lett.* **85**, 2801 (2000).

37. J. Maly, B. Jankó, and K. Levin, *Physica* **C321**, 113 (1999).

38. P.A. Lee, N. Nagaosa, and X.-G. Wen, *preprint, cond-mat/0410445* (unpublished).

39. E.W. Carlson, V.J. Emery, S.A. Kivelson, and D. Orgad, *preprint; cond-mat/0206217* (unpublished).

40. V.M. Loktev, R.M. Quick, and S.G. Sharapov, *Phys. Rep.* **349**, 1 (2001).

41. P. Curty and B. Hans, *Phys. Rev. Lett.* **91**, 257002 (2003).

42. Q.J. Chen, I. Kosztin, B. Jankó, and K. Levin, *Phys. Rev.* **B59**, 7083 (1999).

43. P. Pieri and G.C. Strinati, *Phys. Rev.* **B61**, 15370 (2000).

44. Y. Yanase, J. Takanobu, T. Nomura, H. Ikeda, T. Hotta, and K. Yamada, *Phys. Rep.* **387**, 1 (2003).

45. M. Kugler, O. Fischer, Ch. Renner, S. Ono, and Y. Ando, *Phys. Rev. Lett.* **86**, 4911 (2001).

46. M. Oda, K. Hoya, R. Kubota, C. Manabe, N. Momono, T. Nakano, and M. Ido, *Physica* **C281**, 135 (1997).

47. J.W. Loram, K. Mirza, J.R. Cooper, W. Liang, and J. Wade, *J. Supercond.* **7**, 243 (1994).

48. J. Stajic, A. Iyengar, K. Levin, B.R. Boyce, and T.R. Lemberger, *Phys. Rev.* **B68**, 024520 (2003).

49. Z. Xu, N.P. Ong, Y. Wang, T. Kakeshita, and S. Uchida, *Nature* **406**, 486 (2000).

50. J. Corson, R. Mallozzi, J. Orenstein, J.N. Eckstein, and I. Bozovic, *Nature* **398**, 221 (1999).

51. S. Tan and K. Levin, *Phys. Rev.* **B69**, 064510 (2004).

52. M. Houbiers, R. Ferwerda, H.T.C. Stoof, W. McAlexander, C.A. Sackett, and R.G. Hulet, *Phys. Rev.* **A56**, 4864 (1997).

53. B. DeMarco and D.S. Jin, *Science* **285**, 1703 (1999).

54. K.M. O'Hara, S.L. Hemmer, M.E. Gehm, S.R. Granade, and J.E. Thomas, *Science* **298**, 2179 (2002).

55. J.G.A. Baker, *Phys. Rev.* **C60**, 054311 (1999).

56. H. Heiselberg, *J. Phys.* **B37**, 141 (2004).

57. K. Itakura, *Nucl. Phys.* **A715**, 859 (2003).

58. P.F. Kolb and U. Heinz, *preprint nucl-th/0305084* (unpublished).

59. H. Heiselberg, *Phys. Rev.* **A63**, 043606 (2001).

60. J. Carlson, S. Chang, V. Pandharipande, and K. Schmidt, *Phys. Rev. Lett.* **91**, 050401 (2003).

61. M. Greiner, C.A. Regal, and D.S. Jin, *Nature* **426**, 537 (2003).

62. C.A. Regal, C. Ticknor, J.L. Bohn, and D.S. Jin, *Nature* **424**, 47 (2003).

63. K.E. Strecker, G.B. Partridge, and R. Hulet, *Phys. Rev. Lett.* **91**, 080406 (2003).

64. J. Cubizolles, T. Bourdel, S. Kokkelmans, G. Shlyapnikov, and C. Salomon, *Phys. Rev. Lett.* **91**, 240401 (2003).

65. S. Jochim, M. Bartenstein, A. Altmeyer, G. Hendl, C. Chin, J.H. Denschlag, and R. Grimm, *Phys. Rev. Lett.* **91**, 240402 (2003).

66. S. Jochim, M. Bartenstein, A. Altmeyer, G. Hendl, S. Riedl, C. Chin, J.H. Denschlag, and R. Grimm, *Science* **302**, 2101 (2003).

67. M.W. Zwierlein, C.A. Stan, C.H. Schunck, S.M.F. Raupach, S. Gupta, Z. Hadzibabic, and W. Ketterle, *Phys. Rev. Lett.* **91**, 250401 (2003).

68. T. Bourdel, L. Khaykovich, J. Cubizolles, J. Zhang, F. Chevy, M. Teichmann, L. Tarruell, S.J. Kokkelmans, and C. Salomon, *Phys. Rev. Lett.* **93**, 050401 (2004).

69. C.A. Regal, M. Greiner, and D.S. Jin, *Phys. Rev. Lett.* **92**, 040403 (2004).

70. M.W. Zwierlein, C.A. Stan, C.H. Schunck, S.M.F. Raupach, A.J. Kerman, and W. Ketterle, *Phys. Rev. Lett.* **92**, 120403 (2004).

71. J. Kinast, S.L. Hemmer, M.E. Gehm, A. Turlapov, and J.E. Thomas, *Phys. Rev. Lett.* **92**, 150402 (2004).

72. C. Chin, M. Bartenstein, A. Altmeyer, S. Riedl, S. Jochim, J.H. Denschlag, and R. Grimm, *Science* **305**, 1128 (2004).

73. F. Dalfovo, S. Giorgini, L.P. Pitaevskii, and S. Stringari, *Rev. Mod. Phys.* **71**, 463 (1999).

74. M. Bartenstein, A. Altmeyer, S. Riedl, S. Jochim, C. Chin, J.H. Denschlag, and R. Grimm, *Phys. Rev. Lett.* **92**, 120401 (2004).

75. M. Bartenstein, A. Altmeyer, S. Riedl, S. Jochim, C. Chin, J.H. Denschlag, and R. Grimm, *Phys. Rev. Lett.* **92**, 203201 (2004).

76. J. Kinnunen, M. Rodriguez, and P. Törmä, *Science* **305**, 1131 (2004).

77. J. Kinast, A. Turlapov, J.E. Thomas, Q.J. Chen, J. Stajic, and K. Levin, *Science* **307**, 1296 (2005), published online 27 January 2005; doi:10.1126/science.1109220.

78. M.W. Zwierlein, J.R. Abo-Shaeer, A. Schirotzek, and W. Ketterle, *Nature* **435**, 170404 (2005).

79. Q.J. Chen, J. Stajic, S.N. Tan, and K. Levin, *Phys. Rep.* **412**, 1 (2005).

80. T. Kostyrko and J. Ranninger, *Phys. Rev.* **B54**, 13105 (1996).

81. R. Friedberg and T.D. Lee, *Phys. Lett.* **A138**, 423 (1989).

82. T. Friedberg and T.D. Lee, *Phys. Rev.* **B40**, 6745 (1989).

83. V. Geshkenbein, L. Ioffe, and A. Larkin, *Phys. Rev.* **B55**, 3173 (1997).

84. J.W. Serene, *Phys. Rev.* **B40**, 10873 (1989).

85. R. Haussmann, *Z. Phys.* **B91**, 291 (1993).

86. O. Tchernyshyov, *Phys. Rev.* **B56**, 3372 (1997).

87. L.P. Kadanoff and P.C. Martin, *Phys. Rev.* **124**, 670 (1961).

88. A. Perali, P. Pieri, and G.C. Strinati, *Phys. Rev. Lett.* **93**, 100404 (2004).

89. J. Stajic, A. Iyengar, Q.J. Chen, and K. Levin, *Phys. Rev.* **B68**, 174517 (2003).

90. I. Kosztin, Q.J. Chen, Y.-J. Kao, and K. Levin, *Phys. Rev.* **B61**, 11662 (2000).

91. J. Stajic, Q.J. Chen, and K. Levin, *Phys. Rev.* **A71**, 033601 (2005).

92. Q.J. Chen, J. Stajic, and K. Levin, *arXiv:cond-mat/0411090* (unpublished).

93. J. Stajic, Q.J. Chen, and K. Levin, *Phys. Rev. Lett.* **94**, 060401 (2005).

94. J. Kinnunen, M. Rodriguez, and P. Törmä, *Phys. Rev. Lett.* **92**, 230403 (2004).

95. Y. He, Q.J. Chen, and K. Levin, *Phys. Rev.* **A72**, 011602(R) (2005).

96. J. Kinast, A. Turlapov, and J.E. Thomas, *Phys. Rev. Lett.* **94**, 170404 (2005).

97. A. Perali, P. Pieri, L. Pisani, and G.C. Strinati, *Phys. Rev. Lett.* **92**, 220404 (2004).

98. T.-L. Ho, *Phys. Rev. Lett.* **92**, 090402 (2004).

99. J. Kinast, A. Turlapov, and J.E. Thomas, *preprint cond-mat/0409283* (unpublished).

100. M.L. Chiofalo, S.J.J.M.F. Kokkelmans, J.N. Milstein, and M.J. Holland, *Phys. Rev. Lett.* **88**, 090402 (2002).

101. H. Hu, A. Minguzzi, X.-J. Liu, and M.P. Tosi, *Phys. Rev. Lett.* **93**, 190403 (2004), see also the preprint version, *cond-mat/0404012* v1. The transverse breathing mode data from Bartenstein et al. shown in Fig. 2 of the published version has recently been corrected so that they agree with both theory and the data from Kinast et al.

102. H. Heiselberg, *Phys. Rev. Lett.* **93**, 040402 (2004).

103. J. Kinast, A. Turlapov, and J.E. Thomas, *Phys. Rev.* **A70**, 051401(R) (2004).

104. C. Chin and R. Grimm, *private communication*.

105. S. Stringari, *Europhys. Lett.* **65**, 749 (2004).

106. J.R. Schrieffer, *Theory of Superconductivity*, Perseus Books, Reading, MA (1983).

107. S. Tan and K. Levin, *arXiv:cond-mat/0506293* (unpublished).

108. D.S. Petrov, C. Salomon, and G.V. Shlyapnikov, *Phys. Rev. Lett.* **93**, 090404 (2004).

109. M.J. Holland, C. Menotti, and L. Viverit, *preprint, cond-mat/0404234* (unpublished).

110. M. Greiner, C.A. Regal, and D.S. Jin, *Phys. Rev. Lett.* **94**, 070403 (2005).

111. G.B. Partridge, K.E. Strecker, R.I. Kamar, M.W. Jack, and R.G. Hulet, *Phys. Rev. Lett.* **95**, 020404 (2005).

112. Q.J. Chen and K. Levin, *arXiv:cond-mat/0505689* (unpublished).

113. J.W. Loram, K.A. Mirza, J.R. Cooper, and J.L. Tallon, *J. Phys. Chem. Solids* **59**, 2091 (1998).

114. R.X. Liang, D.A. Bonn, W.N. Hardy, and B.D, *Phys. Rev. Lett.* **94**, 117001 (2005).

115. Q.J. Chen, K. Levin, and I. Kosztin, *Phys. Rev.* **B63**, 184519 (2001).

116. Y. Zuev, M.S. Kim, and T. Lemberger, *arXiv:cond-mat/0410135* (unpublished).

117. P.A. Lee and X.-G. Wen, *Phys. Rev. Lett.* **78**, 4111 (1997).

118. A. Iyengar, J. Stajic, Y.-J. Kao, and K. Levin, *Phys. Rev. Lett.* **90**, 187003 (2003).

119. Q.J. Chen and J.R. Schrieffer, *Phys. Rev.* **B66**, 014512 (2002).

120. Y.-J. Kao, A. Iyengar, J. Stajic, and K. Levin, *Phys. Rev.* **B68**, 214519 (2002).

121. Y.-J. Kao, A. Iyengar, Q.J. Chen, and K. Levin, *Phys. Rev.* **B64**, 140505 (2001).